Energy 290 (2024) 129969

Contents lists available at ScienceDirect

Energy

journal homepage: www.elsevier.com/locate/energy

Digital twin modeling and operation optimization of the steam turbine system of thermal power plants

Chen Chen, Ming Liu *, Mengjie Li, Yu Wang, Chaoyang Wang, Junjie Yan

State Key Laboratory of Multiphase Flow in Power Engineering, Xi'an Jiaotong University, Xi'an, 710049, China

ARTICLE INFO

Handling Editor: Ruzhu Wang

Keywords:
Thermal power plant
Steam turbine system
Digital twin
Water-coal ratio
Operation optimization

ABSTRACT

The increasing deployment of renewable energy sources necessitates peak regulation services from thermal power plants, impacting their energy efficiency. Central to these plants, the steam turbine system significantly influences their operational efficiency. A digital twin model of this system was developed, integrating mechanism-driven and data-driven modeling methods. The neural network data-driven approach was specifically utilized for parameters such as feedwater pump speed and steam flow rate to the pump turbine. Other parameters were modeled with mechanism data hybrid driven modeling method. This model computes vital metrics such as low-pressure turbine exhaust steam enthalpy, work done and heat absorption per unit mass of steam, system efficiency, feedwater mass flow rate, and water-coal ratio—key for evaluating and enhancing the system's energy efficiency. An investigation into a reference case showed a decline in efficiency below design levels due to aging. By optimizing the live steam pressure and the cold-end system, relative improvements in energy efficiency of 0.35 % and 0.14 %, respectively, were achievable.

1. Introduction

To attain sustainable development, the global energy supply is transitioning from fossil fuel dominance to a prevalence of low-carbon energy sources, with a notable surge in the development of renewable energy sources, particularly wind and solar power [1]. In many developing nations, coal power serves as the primary source for electricity generation [2–4]. Consequently, coal power plants are increasingly tasked with providing peaking shaving services to accommodate the intermittent and variable output of renewable power sources [5,6]. Furthermore, advancements in energy-saving technologies for thermal power plants are crucial to reduce carbon emissions [7]. Consequently, optimizing the operation of thermal power plants to achieve reliability, cost efficiency, and flexibility represents a pivotal facet of thermal power technology advancement [8].

Digitization has emerged as an efficacious avenue for optimizing the operation of thermal power plants, with the concept of “smart power plants” playing a crucial role in enhancing operational reliability, cost efficiency, and flexibility [9]. The digital twin technique facilitates the connection between the physical power plant and its digital counterpart [10]. It serves as a foundational technique for the construction of smart power plants. Originating in 2003 through the work of Professor Michael Grieves, the digital twin concept represents an advanced technique that integrates attributes spanning multiple physical aspects, scales, and disciplines [11,12]. Leveraging digital tools, physical entities are replicated or twinned in a virtual environment [13]. Digital twin modeling is based on the concept of digital twin, using a variety of data-driven modeling methods, combined with the physical mechanism of each equipment, to accurately model the simulation object. The digital power plant model enables real-time monitoring of essential performance parameters, economic metrics, and safety indicators for thermal power plants, thereby enhancing the flexibility of thermal units to swiftly respond to the demands of peak and frequency regulation within the power grid. This leads to increased load change rates, decreased steady-state loads, and improved thermal efficiency under variable loads. Consequently, the application of digital twin modeling to thermal power plants proves both beneficial and essential [14].

Regarding the digital twin modeling of thermal power plants, research primarily follows a three-phase progression including big data analysis, digital modeling, and operation optimization. Data analysis constitutes the foundational phase of digital twin modeling. Mao et al. [15] conducted significant research on the optimization of thermal power plants using big data, culminating in the development of a multisource heterogeneous data integration model for power plant performance information. This model supports both online and offline

* Corresponding author.
E-mail address: ming.liu@mail.xjtu.edu.cn (M. Liu).

https://doi.org/10.1016/j.energy.2023.129969
Received 18 September 2023; Received in revised form 24 November 2023; Accepted 8 December 2023
Available online 17 December 2023
0360-5442/© 2023 Elsevier Ltd. All rights reserved.

Nomenclature

Abbreviations

B-MCR	boiler maximum continuous rating
BP	booster pump
CP	condensate pump
DCS	distributed control system
FP	feedwater pump
FPT	feedwater pump turbine
HPT	high-pressure turbine
IPT	intermediate pressure turbine
LPT	low-pressure turbine
PCA	principal component analysis
RH	regenerative heater
STS	steam turbine system

Parameters

H	work done per unit mass of live steam, kJ/kg
H_{bp}	BP head, MPa
H_{fp}	FP head, MPa
H_g	pressure of height difference between deaerator and FP, MPa
H_i, H_r	equivalent enthalpy drop of extraction steam of the No.i/No.r regenerative heater, kJ/kg
N	FP relative rotary speed
Q	heat absorption per unit mass of live steam, kJ/kg
T_{cwi}	circulating water inlet temperature, °C
W_e	generated power, MW
W_p	FP power consumption rate, kW
W_t	output power of steam turbine, MW
c_1, c_2, c_3, c_4, c_5, c_6	coefficients fitted by the performance characteristic curves
h_c	enthalpy of LPT exhaust steam, kJ/kg
h_{cs}	isentropic enthalpy of LPT exhaust steam, kJ/kg
h_{ept}	steam enthalpy at the FPT outlet, kJ/kg
$h_{in,1}$	enthalpy of feedwater of boiler, kJ/kg
$h_{in,2}$	enthalpy of cold reheat steam, kJ/kg
$h_{out,1}$	enthalpy of live steam, kJ/kg
$h_{out,2}$	enthalpy of hot reheat steam, kJ/kg
$h_{s,i}$	enthalpy of the No.i steam extraction, kJ/kg
h_{spt}	steam enthalpy at the FPT inlet, kJ/kg
k_1, k_2, k_3, k_4, k_5, k_6, k_7, k_8, k_9	coefficients obtained by data fitting of mechanism data hybrid driven modeling
m_c	interspace extraction water flow rate of the FP, kg/s
m_{co}	mass flow rate of coal to the boiler, kg/s
m_{fw}	feedwater mass flow rate at the FP outlet, t/h
m_{fw1}	feedwater mass flow rate at the FP inlet, t/h
$mixi$	the nearest mixing heater with extraction pressure lower than No.i extraction
m_{spt}	mass flow rate of steam to the FPT, t/h
m_w	feedwater mass flow rate of the boiler, kg/s
m_{w1}, m_{w2}	feedwater mass flow rates of different circulating water inlet temperatures, kg/s
m_{wh}	feedwater mass flow rate under the cold end condition of 2 circulating pumps in service, kg/s
p_c	pressure of LPT exhaust steam, kPa
p_{de}	deaerator pressure, MPa
p_{ept}	FPT exhaust steam pressure, kPa
p_{fw}	feedwater pressure at the FP outlet, MPa
p_{ie}	interspace extraction pressure of the FP, MPa
p_{obp}	BP outlet pressure, MPa
$p_{s,6}$	No.6 extraction pressure, MPa
q_{net}	net calorific value of coal, kJ/kg
q_r	heat release per unit mass of extracted steam of the No.r regenerative heater, kJ/kg
α_2	proportion of reheat steam to live steam
γ_r	heat release of the drain water of the No. r regenerative heater, kJ/kg
$\eta_{6\text{-}c}$	isentropic efficiency of LPT pressure stages from the No. 6 steam extraction point to the condenser
η_b	boiler efficiency
η_{fp}	FP efficiency
η_{fptm}	FPT mechanical efficiency
η_g	generator efficiency
η_m	mechanical efficiency
η_{sts}	efficiency of STS
λ	water-coal ratio
λ_1, λ_2	water-coal ratio of different circulating water inlet temperatures
λ_h	water-coal ratio under the cold end condition of 2 circulating pumps in service
σ	heat absorption of the reheated steam in the boiler reheater, kJ/kg
τ_r	enthalpy rise of feedwater in the No. r regenerative heater, kJ/kg
$\sum\prod$	amount of work capacity reduction per unit mass of live steam caused by losses, kJ/kg

Subscripts

ept	exhaust steam at the FPT outlet
ie	interspace extraction
obp	outlet of booster pump
spt	steam at the FPT inlet

distributed analyses. Huang et al. [16] introduced a high-performance distributed computing platform for power systems, enabling knowledge discovery related to power system security through extensive big data analysis. Wang et al. [17] employed the fuzzy rough set method to focus on data-driven modeling of thermal power units.

The development of a reliable, robust, and expeditious simulation model constitutes the central phase of digital twin modeling. Zhao et al. [18,19] established a dynamic simulation model for coal-fired power plants, facilitating an assessment of the effect of various measures on power plant operational flexibility. Alobaid et al. [20] created a dynamic simulation model for a waste heat steam generator, ensuring a dependable response to flue gas transients. Tian et al. [21] devised an online performance monitoring platform grounded in a comprehensive process model of a coal-fired power plant. This platform offers real-time feedback monitoring capabilities and can be employed for offline operational reviews. Numerous comprehensive studies have also been conducted on dynamic modeling, including coal-fired power stations [22], feedwater pump (FP) systems [23–25], condensers [26,27], and water−wall tubes in supercritical boilers [28].

Operation optimization constitutes the ultimate objective of digital twin modeling. Zhang et al. [29] proposed an online optimization method reliant on variable speed pump condenser pressure with circulating water mass flow serving as the control variable, ultimately leading to heightened energy efficiency. Runvik [30] harnessed the JModelica.org platform for the simulation of coal-fired power plants to optimize the startup process. A plethora of comprehensive studies have also been conducted pertaining to the operation optimization of gas-steam combined cycle units [31,32], control strategies based on boiler heat storage characteristics [33], and superheated steam temperature control systems [34].

The steam turbine system (STS) comprises components such as steam turbines, regenerative heaters, FPs, and others, and it plays a pivotal role in determining the energy efficiency of thermal power plants. Numerous comprehensive studies have been conducted to optimize the system [17,30,35], evaluate its performance both offline and online [21,36], and enhance its operational flexibility [18,19,33,37]. However, digital twin modeling of the STS, a method that can assess performance using operational big data and offer guidance for closed-loop control, remains inadequately addressed. To address this research gap, rooted in the principles of digital twin modeling, an STS digital twin model has been developed utilizing a hybrid modeling approach based on mechanisms and data-driven techniques for different digital twin parameters, enabling a comprehensive obtaining of STS energy efficiency and other critical parameters. This study introduces several novel contributions: (1) Two distinct digital twin simulation methods are presented for parameters related to STS energy efficiency: a mechanism data hybrid driven modeling method and a neural network data-driven modeling method. (2) An online energy efficiency analysis model for the STS has been developed through a hybrid modeling approach that combines mechanism-driven and data-driven techniques. This model can evaluate, diagnose, and optimize the energy efficiency of the STS. (3) The STS digital twin model facilitates live steam pressure optimization and cold end optimization, offering valuable guidance for closed-loop control.

In this paper, we commence by collecting and cleansing operational big data from thermal power plants. Subsequently, we provide two digital twin modeling methods, namely, the mechanism data hybrid driven modeling method and the neural network data-driven modeling method, tailored to the characteristics of different parameters associated with STS energy efficiency. Using the mechanism data hybrid driven modeling method, we obtain simulation data for six crucial digital twin parameters, including booster pump (BP) outlet pressure, feedwater mass flow rate of the FP, FP outlet pressure, FP efficiency, FP power, and exhaust steam pressure of the feedwater pump turbine (FPT). Meanwhile, the neural network data-driven modeling method is employed to simulate the FP's relative rotary speed and the mass flow rate of steam to the FPT, ensuring high accuracy.

Next, we develop an online energy efficiency analysis model for the STS through a hybrid modeling approach that integrates mechanism-driven and data-driven methods. This energy efficiency analysis model yields simulation data for six vital parameters that influence or reflect STS energy efficiency. These parameters include exhaust steam enthalpy of low-pressure turbine(LPT), work done per unit mass of working medium, heat absorption per unit mass of working medium, STS energy efficiency, feedwater mass flow rate, and water-coal ratio. Additionally, we examine the effect of varying circulating water inlet temperatures on STS energy efficiency.

Finally, after diagnosing the STS energy efficiency, we conduct live steam pressure optimization and cold end optimization, taking into account different live steam pressures and the number of circulating pumps in service.

2. Model development

In this section, we outline the digital twin modeling procedure utilizing a hybrid approach that combines mechanism-driven and data-driven methods. Subsequently, we will investigate the specific digital twin parameters of the FP subsystem, which exert a significant influence on the energy efficiency of the STS. Finally, we will develop an online energy efficiency analysis model for the STS and derive an online water-coal ratio curve. This curve serves as a valuable tool for guiding operational optimization based on the STS digital twin model.

2.1. Digital twin modeling procedure of the STS

Fig. 1 illustrates the temperature-entropy (T-S) diagram for the ultra-supercritical Rankine cycle of the reference unit. This reference unit

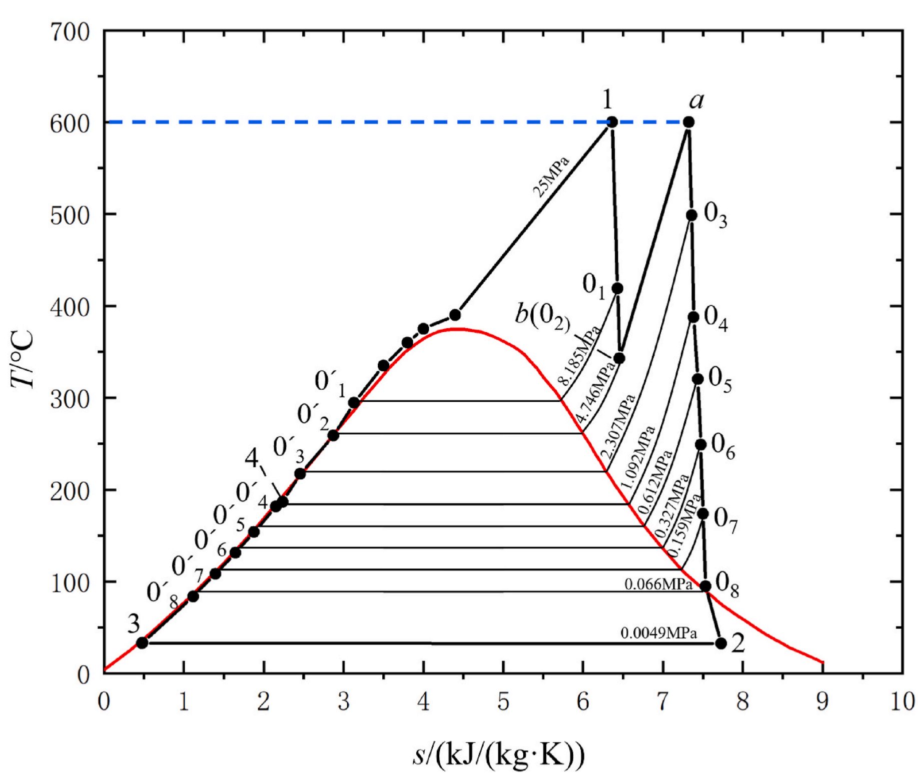

Fig. 1. The *T-S* diagram of the ultra-supercritical Rankine cycle.
1-*b* adiabatic expansion at high pressure turbine; *b*-*a* reheating; *a*-2 adiabatic expansion at intermediate pressure turbine and low pressure turbine; 0_1, 0_2, 0_3, 0_4, 0_5, 0_6, 0_7, 0_8 steam turbine extraction; 2-3 isobaric heat release; 3-$0'_1$ heat absorption at regenerative heaters; $0'_4$-4 adiabatic compression; $0'_1$, $0'_2$, $0'_3$, $0'_4$, $0'_5$, $0'_6$, $0'_7$, $0'_8$ feedwater in regenerative system; $0'_1$-1 isobaric heat absorption at the boiler.

boasts a capacity of 1030 MW and operates as an ultra-supercritical, once-through, intermediate reheating system equipped with eight regenerative heaters. It maintains a rated main steam pressure of 25 MPa and a rated reheated steam pressure of 4.366 MPa. Both the rated main steam temperature and reheated steam temperature are set at 600 °C. The feedwater system is powered by two 50 % Base Maximum Continuous Rating (B-MCR) steam-driven FPs, complemented by one 30 % B-MCR standby electric pump.

Fig. 2 outlines the modeling scope of the STS. The STS includes several key components, including steam turbines (comprising the high pressure turbine (HPT), intermediate pressure turbine (IPT), low pressure turbine (LPT), and feedwater pump turbine (FPT), regenerative heaters (denoted as No.1 to No.8 Regenerative Heaters), and pumps (comprising the condensate pump, booster pump, and FP). The operational sequence involves the live steam entering the HPT to perform work, subsequently proceeding to the boiler reheater for reheating. The hot reheat steam then enters the IPT to perform additional work before ultimately being discharged into the condenser. The condensate water undergoes successive heating stages facilitated by the regenerative heaters, progressing from No. 8 to No. 1 Regenerative Heaters.

Energy efficiency is a pivotal concern in the operation of STSs and is inherently reflected in operational parameters, which necessitate digital modeling. The FP subsystem, comprising the FPT, BP, and FP, plays a central role in supplying feedwater to the boiler while consuming a substantial amount of power. Consequently, the energy efficiency of this subsystem significantly impacts the overall energy efficiency of the STS.

Key parameters of the FP subsystem that exert a substantial influence on the energy efficiency of the STS include the following: deaerator pressure (p_{de}), BP outlet pressure (p_{obp}), feedwater mass flow rate of the FP (m_{fw}), feedwater pressure at the FP outlet (p_{fw}), FP relative rotary speed (N), FP efficiency (η_{fp}), FP power consumption rate (W_p), mass flow rate of steam to the FPT (m_{spt}) and FPT exhaust steam pressure (p_{ept}). Additionally, several pivotal parameters serve as indicators of the energy efficiency of the STS, including the enthalpy of LPT exhaust steam (h_c), work done per unit mass of live steam (H), absorption per unit mass of live steam (Q), energy efficiency of STS (η_{sts}), mass flow rate of feedwater (m_w), and water-coal ratio (λ).

Henceforth, the crucial parameters governing the energy efficiency of the STS will be subjected to digital twin modeling methods. The digital twin modeling procedure is elucidated in Fig. 3. In the process of selecting measurement data, we strictly followed the criterion of the power variation rate below 0.25 % per minute to meet the requirements of steady-state modeling. And all data needed for digital twin modeling are acquired from the distributed control system of the thermal power plant, facilitating the development of an energy efficiency analysis model for the STS. A Distributed Control System (DCS) is an automated control system widely used in the thermal power plants, which consists of distributed controllers, central control room, data acquisition and processing, alarm and event logging and data storage.

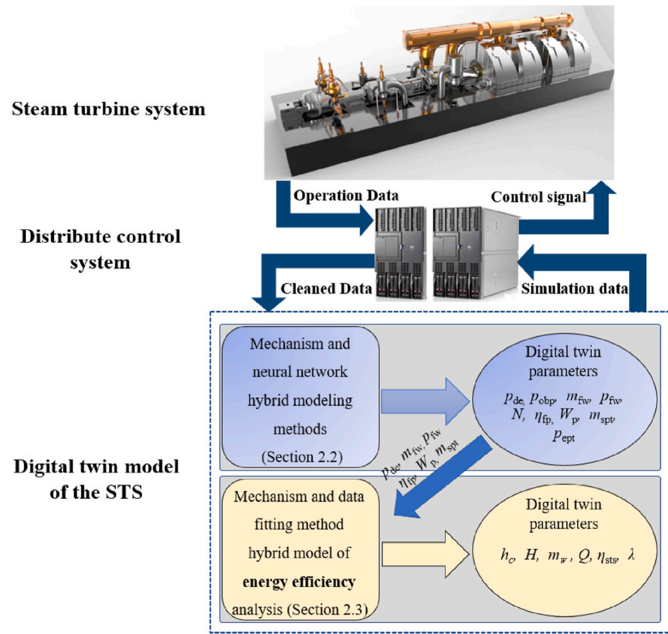

Fig. 3. Digital twin modeling procedure of the STS.

The pertinent digital twin parameters of the FP subsystem, which significantly influence the STS energy efficiency, are extracted using the mechanism data hybrid modeling method. Parameters including the deaerator pressure (p_{de}), feedwater mass flow rate of the FP (m_{fw}), feedwater pressure at the FP outlet (p_{fw}), FP efficiency (η_{fp}), FP power consumption rate (W_p), mass flow rate of steam to the FPT (m_{spt}) and others are supplied to the energy efficiency analysis model of the STS.

Subsequently, the energy efficiency analysis model of the STS computes parameters such as the enthalpy of LPT exhaust steam (h_c), the work done per unit mass of live steam (H), the heat absorption per unit mass of live steam (Q), the energy efficiency of STS (η_{sts}), and the feedwater mass flow rate (m_w), which are obtained by the energy efficiency analysis model of the STS. Ultimately, the water-coal ratio (λ)

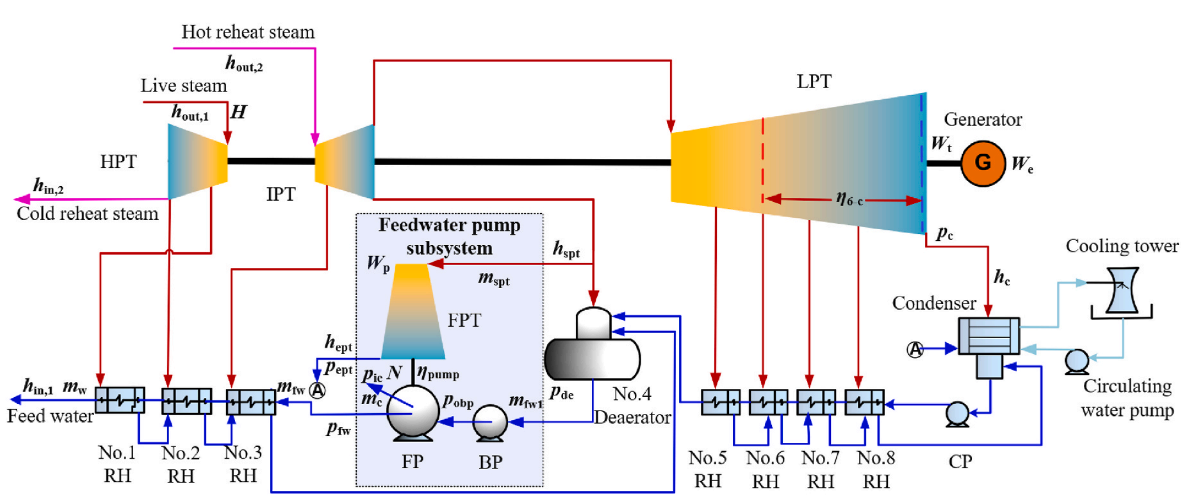

Fig. 2. Modeling scope of the steam turbine system.
HPT-high pressure turbine, IPT-intermediate pressure turbine, LPT-low pressure turbine, FPT-feedwater pump turbine, RH-regenerative heater, FP-feedwater pump, CP-condensate pump, BP-booster pump.

under varying output power conditions of the thermal power plant can be determined and relayed to the distributed control system for precise control, thereby enhancing the overall energy efficiency of the STS.

2.2. Modeling methods for digital twin parameters

The significant digital twin parameters of the FP subsystem, which wield substantial influence over the energy efficiency of the STS, are derived through a hybrid modeling method combining mechanism data hybrid driven and neural networks. This section will elucidate the modeling methods employed in obtaining these crucial parameters.

2.2.1. Mechanism data hybrid driven modeling

The mass flow rate of live steam maintains an approximately linear relationship with the unit's power output, so the feedwater mass flow rate is almost linearly correlated with the unit's power output. The feedwater mass rate of the FP can be computed as follows:

$$m_{\mathrm{fw}} = k_1 W_{\mathrm{e}} + k_2 \tag{1}$$

where m_{fw} is the feedwater mass rate of the FP, t/h; W_{e} is the output power of the thermal power plant, MW; and the coefficients k_1 and k_2 are determined through fitting with historical data between m_{fw} and W_{e}. In Eq. (1), the primary determinants for k_1 and k_2 are the unit's steam consumption rate. This rate, in turn, is contingent upon the specific structural and parameter design of both the boiler and steam turbine, in addition to the unit's operational load.

Considering the essentially linear association between the feedwater pressure at the FP outlet and the feedwater mass flow rate, the relation of the feedwater pressure at the FP outlet with the unit's power output is

$$p_{\mathrm{fw}} = k_3 W_{\mathrm{e}} + k_4 \tag{2}$$

where p_{fw} is the outlet pressure of the FP, MPa. The coefficients k_3 and k_4 are determined through fitting with historical data of p_{fw} and W_{e}. In Eq. (2), k_3 and k_4 describe the relationship between the unit's load and the FP outlet pressure. Therefore, k_3 and k_4 are mainly associated with the live steam pressure control strategies during load variations.

In accordance with the actual performance characteristic curve of the FP, the relationship between the FP head and the mass flow rate at the rated rotary speed can be represented as follows [38]:

$$H_{\mathrm{fp}} = c_1 + c_2 m_{\mathrm{fw}} + c_3 {m_{\mathrm{fw}}}^2 \tag{3}$$

where H_{fp} is the FP head, MPa; The parameters c_1, c_2, and c_3 in Eq. (3) are primarily derived from fitting the performance characteristics of the FP provided by the pump manufacturer, which is obtained at its rated speed. These parameters are closely associated with the design of pump, and can also be utilized for head calculations at different speeds due to the similarity law of pump as

$$H_{\mathrm{fp}} = c_1 N^2 + c_2 N m_{\mathrm{fw}} + c_3 {m_{\mathrm{fw}}}^2 \tag{4}$$

where N is the FP relative rotary speed.

The FP relative rotary speed can be evaluated with:

$$N = k_5 \frac{\left(-c_2 m_{\mathrm{fw}} + \sqrt{\left(c_2 m_{\mathrm{fw}}\right)^2 - 4c_1\left(c_3 {m_{\mathrm{fw}}}^2 - H_{\mathrm{fp}}\right)} \right)}{2c_1} \tag{5}$$

where k_5 is the performance attenuation correction coefficient of FP. In Eq. (5), the parameter k_5 describes the degradation of the FP performance. This coefficient is associated with the FP performance design data and its degradation condition.

Similar to the relationship between the FP head and the feedwater flow rate of the FP, based on the actual performance characteristic curve of the FP and the water pump similarity law, the correlation between FP efficiency, feedwater mass flow rate, and rotational speed can be articulated as follows [39]:

$$\eta_{\mathrm{fp}} = c_4 + c_5 \left(\frac{m_{\mathrm{fw}}}{N}\right) + c_6 \left(\frac{m_{\mathrm{fw}}}{N}\right)^2 \tag{6}$$

where η_{fp} is the FP efficiency; Eq. (6) involves c_4, c_5, and c_6, which depict the relationship between the feedwater mass flow rate and the FP efficiency. These coefficients are determined by fitting the relationship between η_{fp} and m_{fw} at the rated speed provided by the FP manufacturer. c_4, c_5, and c_6 are primarily linked to the FP inherent performance.

Below are characteristic curves illustrating the relationship between FP efficiency and flow rate for FP relative rotary speeds of 1.0, 0.8, 0.6, and 0.4, as depicted in Fig. 4. To sustain a high efficiency across a range of feedwater mass flow rates, the FP must operate at different rotary speeds.

The coefficients within Eq. (6) remain applicable even as the relative rotary speed of the FP varies, thanks to the principles governed by pump similarity laws. However, it is crucial to acknowledge that Eq. (6) holds true under the assumption that the FP has not experienced significant performance degradation since its initial commissioning. In cases where the pump undergoes substantial performance degradation or significant alterations to its physical structure, adjustments become necessary.

Taking into account the unit conversion and standardization of both the FP head and feedwater mass flow rate, we can provide the following equation for calculating the power consumed by the FP [40]:

$$W_{\mathrm{p}} = \frac{10^3 H_{\mathrm{fp}}}{\rho g} \times \frac{m_{\mathrm{fw}} g}{3.6} \times \frac{1}{\eta_{\mathrm{fp}}} = \frac{10^3 H_{\mathrm{fp}} m_{\mathrm{fw}}}{3.6 \rho \eta_{\mathrm{fp}}} \tag{7}$$

where W_{p} is the power consumed by the FP, kW; ρ is the fluid density, kg/m^3; g is the acceleration of gravity, m/s^2; and 1/3.6 is the unit conversion factor from kg/s to t/h.

Then, the mass flow rate of steam to the FPT [41] is

$$m_{\mathrm{spt}} = \frac{W_{\mathrm{p}}}{\left(h_{\mathrm{spt}} - h_{\mathrm{ept}}\right)\eta_{\mathrm{fptm}}} \times 3.6 \tag{8}$$

where m_{spt} is the mass flow rate of steam to the FPT, t/h; h_{spt} is the steam enthalpy at the FPT inlet, kJ/kg; h_{ept} is the steam enthalpy at the FPT outlet, kJ/kg; η_{fptm} is the FPT mechanical efficiency; and 3.6 is the unit conversion factor from kg/s to t/h.

The FPT exhaust pressure is the sum of the condenser pressure and the pressure loss of the exhaust pipe. The relationship between pressure loss and exhaust flow rate is linearly simplified. Therefore, the FPT exhaust pressure can be represented as

$$p_{\mathrm{ept}} = k_6 m_{\mathrm{spt}} + k_7 + p_{\mathrm{c}} \tag{9}$$

where p_{ept} is the FPT exhaust steam pressure, kPa. The coefficients k_6 and k_7 are determined through fitting with historical data of p_{ept} and m_{spt}. In Eq. (9), k_6 and k_7 describe the relationship between the pressure loss in the FPT exhaust pipe and the exhaust steam mass flow rate. These two coefficients are influenced by the geometric dimensions of the exhaust pipe, fluid viscosity, and length of the pipe.

The FP is divided into two parts by interspace water extraction, and the relationship of flows between the two parts is:

$$m_{\mathrm{fw}} = m_{\mathrm{fw1}} - m_{\mathrm{c}} \tag{10}$$

where m_{fw1} is the inlet water mass flow rate of the FP, t/h; m_{c} is the interspace extraction water flow rate of the FP, t/h.

The relationship of the BP head with the mass flow rate can be obtained according to the BP design data with

$$H_{\mathrm{bp}} = f\left(m_{\mathrm{fw1}}\right) \tag{11}$$

where H_{bp} is the BP head, MPa.

The BP outlet pressure is related to the deaerator pressure and the BP head as:

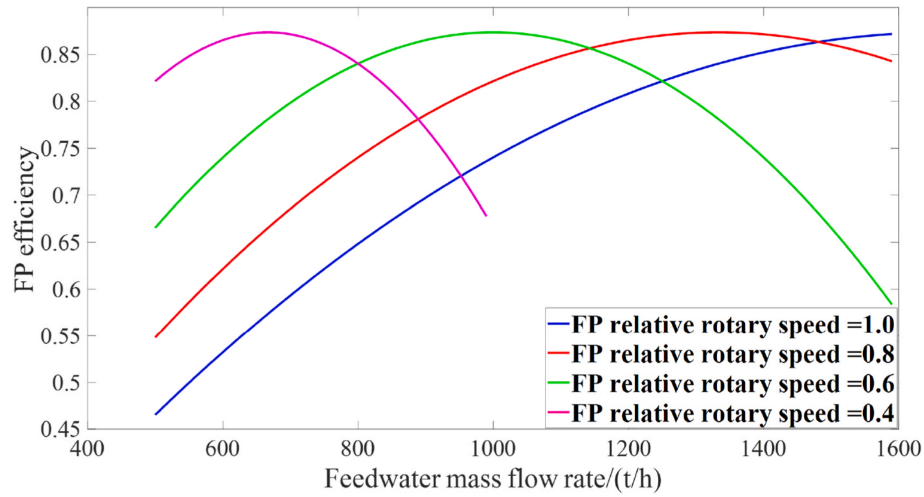

Fig. 4. FP efficiency with different FP relative rotary speeds.

$$p_{\mathrm{obp}} = p_{\mathrm{de}} + H_{\mathrm{bp}} + H_{\mathrm{g}} \tag{12}$$

where p_{obp} is the BP outlet pressure, MPa; p_{de} is the deaerator pressure, MPa; and H_{g} is the height difference between the deaerator and FP, MPa.

The live steam mass flow rate exhibits an approximately linear relationship with the generated power of the thermal power plant, and the steam extraction pressure demonstrates a similar relationship with the live steam mass flow rate. Consequently, the deaerator pressure can be assessed based on the output power of the thermal power plant as follows:

$$p_{\mathrm{de}} = k_8 W_{\mathrm{e}} + k_9 \tag{13}$$

where the coefficients k_8 and k_9 are determined through fitting with historical data of p_{de} and W_{e}. Eq. (13) contains k_8 and k_9, which are related to the structural design of the steam turbine and the live steam pressure control strategies during load changes in the power plant.

2.2.2. Neural network data-driven modeling

The FP relative rotary speed, steam mass flow rate to the FPT, and FPT exhaust pressure are important parameters that influence the secure and efficient operation of the FP subsystem. High simulation accuracy for these parameters is important to optimize the operation of the FP subsystem and the STS. The mechanism-driven modeling method relies on the physical mechanisms of each device, and utilizes on-site data as input for simulation. Its accuracy is constrained by both measurement data and equipment performance degradation. In contrast, the neural network data-driven modeling leverages machine learning with extensive on-site measurement data for multiple parameters. This approach effectively identifies performance degradation in various devices and mitigates the error accumulation issues that may arise in the mechanism-driven modeling process. Therefore, it is necessary to employ the neural network data-driven modeling method to model these three parameters. As illustrated in Fig. 5, the process begins with the compilation of input parameters related to the parameters to be predicted, forming the original dataset after data preprocessing. Subsequently, the original dataset undergoes dimensionality reduction through principal component analysis (PCA). The resulting dataset, post-dimensionality reduction, along with the data pertaining to the output parameters, serves as the input and output parameters, respectively, for training the neural network.

The simulation of FP relative rotary speed involves three input parameters: generated power, mass flow rate and pressure of interspace water extraction. Meanwhile, the simulation of the mass flow rate of steam to the FPT includes six input parameters: generated power, the mass flow rate and pressure of interspace water extraction, measured rotary speed of the FP, and enthalpies of the inlet and outlet of the FPT. In the case of simulating the FPT exhaust steam pressure, an additional input parameter, condenser pressure, is included, along with the

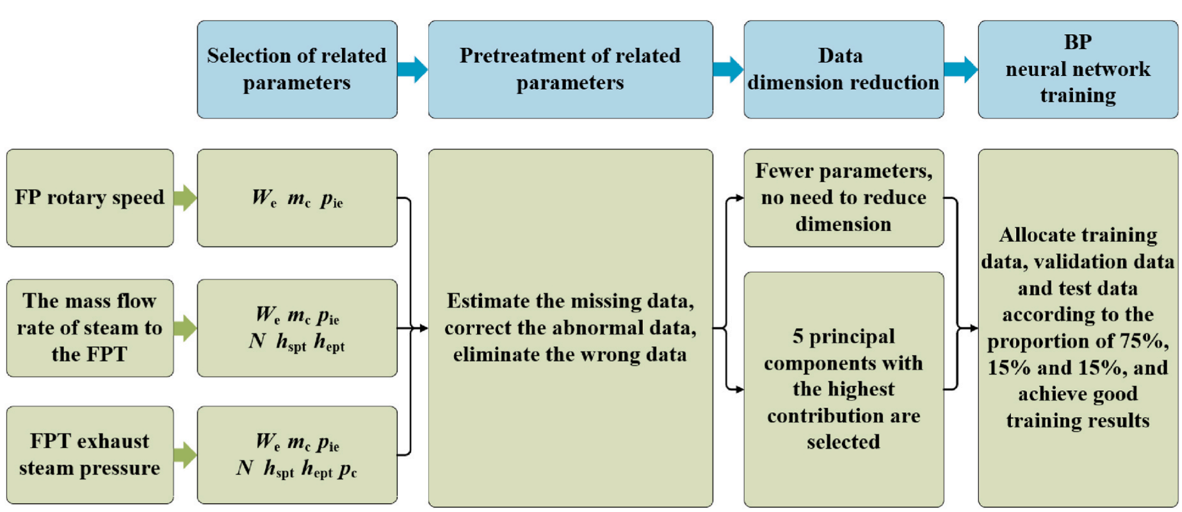

Fig. 5. Flow chart of neural network data-driven modeling.

aforementioned parameters. It is noteworthy that apart from parameters lacking measurement data, the input and target parameters used for neural network training were derived from actual measurements collected at the power plant.

Many of these input parameters are interrelated with the mass flow rate of steam to the FPT and the FPT exhaust steam pressure, which results in substantial data storage requirements and computational complexity during neural network training. To mitigate this, dimensionality reduction of the input parameter dataset through PCA is essential to accelerate neural network training [42].

PCA is a widely employed dimensionality reduction algorithm in the domains of data mining and machine learning. It streamlines datasets, reducing their size and processing complexity, while preserving essential characteristics and meaningful information from the original high-dimensional data. In the PCA process, principal components are selected based on the requirement of data dimension reduction, considering the cumulative contribution of eigenvalues from largest to smallest of the covariance matrix. A transformation matrix is derived based on the number of selected principal components, and in the final step, a new data matrix composed of principal components is obtained by multiplying the original data matrix (after mean subtraction) with the transformation matrix. For the datasets related to the mass flow rate of steam to the FPT and FPT exhaust steam pressure, the top 5 principal components, which make the most significant contributions, are selected. Consequently, the new data matrix is formed using these principal components, effectively achieving data dimension reduction.

Machine learning has been widely applied to optimize thermal systems [43–45]. The back propagation neural network, a multilayer feedforward neural network trained using the error backpropagation algorithm, offers key advantages such as broad applicability, nonlinear modeling capabilities, adaptive learning, a multilayer structure, high parallel processing capability, and a degree of robustness [46].

The back propagation neural network is selected in this study. After applying PCA to reduce data dimensionality, a new data matrix is created with 200,000 datasets, which serves as the training dataset. Within this dataset, 70 % of the data are allocated for training, 15 % for validation, and the remaining 15 % for testing. The neural network architecture features a hidden layer with ten neurons. Three separate neural networks are trained, each with FP relative rotary speed, the mass flow rate of steam to the FPT, and FPT exhaust steam pressure as targets, corresponding to their respective influencing parameters as inputs. The objective is to predict these three parameters as outputs.

As demonstrated in Fig. 6, the regression values (R) of the training data, validation data, and test data of the neural network with different parameters are close to 1, indicating a strong correlation between the predicted output and the target output. These results signify the effectiveness of the training process, yielding accurate predictions.

2.3. Energy efficiency analysis model of the steam turbine system

In this section, we will develop the energy efficiency analysis model for the STS. One crucial parameter for monitoring the energy efficiency is the enthalpy of the LPT exhaust steam. To calculate the enthalpy of the LPT exhaust steam, which is in a saturated steam state, we employ the cubic spline interpolation method to fit the efficiency with the pressure ratio. η_{6-c} is the isentropic efficiency of the LPT pressure stages from the No. 6 steam extraction point to the condenser, as depicted in Fig. 1. We utilize the ratio $p_c/p_{s,6}$, where p_c is the LPT exhaust steam pressure and $p_{s,6}$ is the pressure at extraction point No. 6, to establish a fitting relationship for the isentropic efficiency η_{6-c}. Then, the enthalpy of the LPT exhaust steam can be derived from the operational parameters as follows:

$$h_c = h_{s,6} - \eta_{6-c}\left(h_{s,6} - h_{cs}\right) \tag{14}$$

where h_c is the LPT exhaust steam enthalpy, kJ/kg; $h_{s,6}$ is the enthalpy of the No. 6 steam extraction, kJ/kg; and h_{cs} is the isentropic enthalpy of the LPT exhaust steam, kJ/kg.

Then, the work done per unit mass of live steam is:

$$H = h_{out,1} + \sigma - h_c - \sum_{r=1}^{8} \tau_r \frac{H_r}{q_r} - \sum\prod \tag{15}$$

where $h_{out,1}$ is the live steam enthalpy, kJ/kg; σ is heat absorption of the reheated steam in the boiler reheater, kJ/kg; τ_r is the enthalpy rise of feedwater in the No. r regenerative heater, kJ/kg; H_r is the equivalent enthalpy drop of extraction steam of the No. r regenerative heater, kJ/kg; q_r is heat release per unit mass of extracted steam of the No. r regenerative heater, kJ/kg; and $\sum\prod$ is the amount of work capacity reduction per unit mass of live steam caused by losses, kJ/kg.

The calculation method of the equivalent heat drop H of the extraction steam to the regenerative heater after reheating is:

$$H_i = \left(h_{s,i} - h_c\right) - \left(\sum_{r=i}^{mixi} \frac{\gamma_r}{q_r} H_r + \sum_{r=mixi+1}^{8} \frac{\tau_r}{q_r} H_r\right) \tag{16}$$

and before reheating, it is:

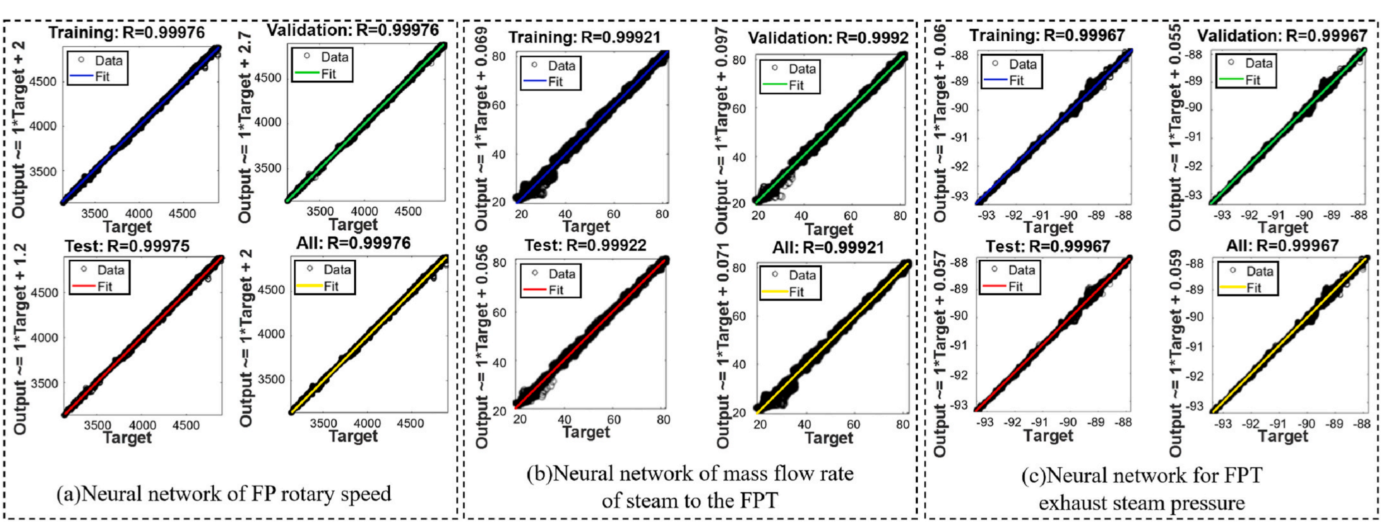

Fig. 6. Regression values R of each neural network dataset.

$$H_i = (h_{s,i} + \sigma - h_c) - \left(\sum_{r=i}^{4} \frac{\gamma_r}{q_r} H_r + \sum_{r=5}^{8} \frac{\tau_r}{q_r} H_r \right) \tag{17}$$

where $h_{s,i}$ is the enthalpy of the No. i steam extraction, kJ/kg; γ_r is the heat release of the drain water of the No. r regenerative heater, kJ/kg; and *mixi* is the nearest mixing heater with an extraction pressure lower than the No. i extraction.

The total heat absorption per unit mass of live steam in boiler Q is:

$$Q = h_{out,1} - h_{in,1} + \alpha_2 (h_{out,2} - h_{in,2}) \tag{18}$$

where α_2 is the proportion of the reheat steam to the live steam; $h_{out,2}$ is the enthalpy of hot reheat steam, kJ/kg; and $h_{in,1}$, $h_{in,2}$ is the enthalpy of feedwater and cold reheat steam, kJ/kg.

Then, the energy efficiency of STS can be obtained with the following operation parameters:

$$\eta_{sts} = \frac{H}{Q} \tag{19}$$

The feedwater mass flow rate m_w can be calculated with the work done per unit mass of live steam H as:

$$m_w = \frac{W_e}{\eta_m \eta_g H} \tag{20}$$

where W_e is the generated power of the power plant, MW; η_m is the mechanical efficiency; and η_g is the generator efficiency.

The water-coal ratio is very important for power plant high-efficiency operation and can be calculated with:

$$\lambda = \frac{m_w}{m_{co}} = \frac{m_w}{\frac{m_w Q}{\eta_b q_{net}}} = \frac{\eta_b q_{net}}{Q} \tag{21}$$

where m_{co} is the mass flow rate of coal to the boiler, kg/s; η_b is the boiler efficiency; and q_{net} is the net calorific value of coal, kJ/kg.

Considering the challenge associated with accurately measuring the coal supply mass flow rate in Eq. (21), this challenge is translated into the calculation of boiler efficiency. By utilizing parameters such as the boiler flue gas temperature, boiler efficiency can be determined using a reverse-balancing approach. This, in turn, facilitates the calculation of the coal-to-water ratio.

The water-coal ratio λ and feedwater mass flow rate (m_w) under various power generation conditions of the power plant can be computed using the aforementioned equations. Subsequently, a curve illustrating the relationship between the water-coal ratio λ and the generated power (W_e) of the power plant can be generated based on operational parameters. This curve serves as a valuable tool for enhancing the efficient operation of power plants as follows:

$$\lambda = f(W_e) \tag{22}$$

3. Results and discussion

In this section, we will compare and select digital twin modeling methods for the parameters to be predicted. Subsequently, we will proceed to model the digital twin parameters related to the energy efficiency of the STS. Following this, we will conduct an energy efficiency evaluation of the STS using the digital twin parameters under varying circulating water inlet temperatures. Finally, we will undertake operation optimization based on the digital twin parameters, including live steam pressure optimization and cold end optimization.

3.1. Modeling on digital twin parameters

The digital twin parameters can be accurately predicted using various modeling methods. Specifically, the BP outlet pressure, feedwater mass flow rate of the FP, feedwater pressure at the FP outlet, FP efficiency, and FP power are predicted using mechanism data hybrid driven modeling methods. Fig. 7 illustrates a comparison between the model-predicted data and the measured data for two digital twin parameters. As depicted in Fig. 7, the mechanism data hybrid driven models exhibit a high level of prediction accuracy. When comparing the simulation values to the measured values for the feedwater mass flow rate and feedwater pressure at the FP outlet across 500,000 data points, it becomes evident that the simulation values closely align with the measured values, with relative errors of 1.67 % and 1.11 %, respectively. These results underscore the high accuracy of the developed models.

The prediction of the FP relative rotary speed, mass flow rate of steam to the FPT, and FPT exhaust steam pressure is accomplished through a combination of mechanism data hybrid driven modeling and neural network data-driven modeling methods. Fig. 8 provides a comparison between the model simulation data and the measured data for these three parameters. The simulation results from both the mechanism data hybrid driven models and the neural network data-driven models closely align with the measured data, with average relative errors of 1.7 % and 1.06 %, respectively. These results underscore the high accuracy of both modeling approaches.

An analysis of the deviations between the two modeling methods is conducted, as shown in Fig. 9. Additionally, Table 1 presents the mean absolute error, root mean square error, and determination coefficient of simulation data obtained from both modeling methods.

The average absolute errors for all parameters are significantly smaller than the 3 % of measured values, indicating a robust alignment between the simulated values and the measurements across the load range of the measured data. Furthermore, the low root mean square error and the determination coefficient, which is very close to 1, provide further evidence of the models' exceptional accuracy.

It is noteworthy that in the simulation of the FP relative rotary speed and the mass flow rate of steam to the FPT, the neural network data-driven modeling demonstrates an advantage over the mechanism data hybrid driven modeling. However, in the simulation of the exhaust steam pressure of the FPT, the reverse holds true, indicating that each modeling method has strengths in specific parameter predictions.

In light of the previous discussion, in the ultimate digital twin parameter simulation model, it is advisable to predict the FP relative rotary speed and the mass flow rate of steam to the FPT using the neural network data-driven modeling method, while other parameters can be reliably obtained through the mechanism data hybrid driven modeling method.

3.2. Energy efficiency diagnosis based on digital twin parameters

From a thermodynamic perspective, the energy efficiency of the STS is influenced by both external irreversibilities (heat source and heat sink) and internal exergy irreversibilities. In Section 3.1, we successfully modeled the digital twin parameters that influence exergy destruction due to internal irreversibilities. Now, we can proceed to diagnose the energy efficiency of the STS based on the inlet parameters of the steam turbines and the parameters of steam exhaust.

The energy efficiency of the STS under varying cold end parameters, specifically different circulating water inlet temperatures (T_{cwi}), is presented in Fig. 10. The inlet temperature of the circulating water has a notable effect on the thermal parameters of the LPT exhaust steam, which in turn affects the energy efficiency of the STS. To facilitate analysis, the operation data were divided into two groups, one with a circulating water inlet temperature of 4.5 ± 1 °C and the other with a circulating water inlet temperature of 6.5 ± 1 °C, as shown in Fig. 10 (a).

The changes in LPT exhaust steam pressure, exhaust steam enthalpy, and work done per unit mass of live steam are illustrated in Fig. 10 (b), (c), and (d), respectively. The LPT exhaust steam mass flow rate increases with the unit load, and the cooling capacity of the cold-end system varies due to changes in the scheduling of the circulating water pumps. As a result, the exhaust pressure initially decreases and

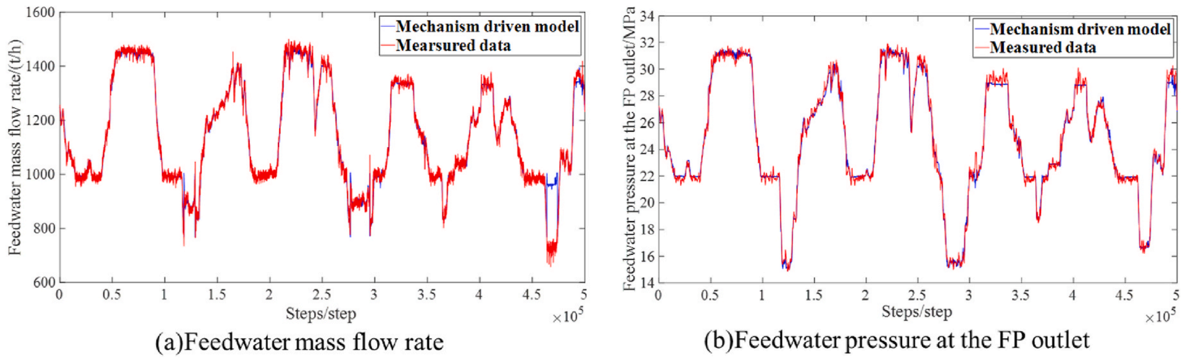

Fig. 7. Parameters only predicted by the mechanism data hybrid driven modeling method.

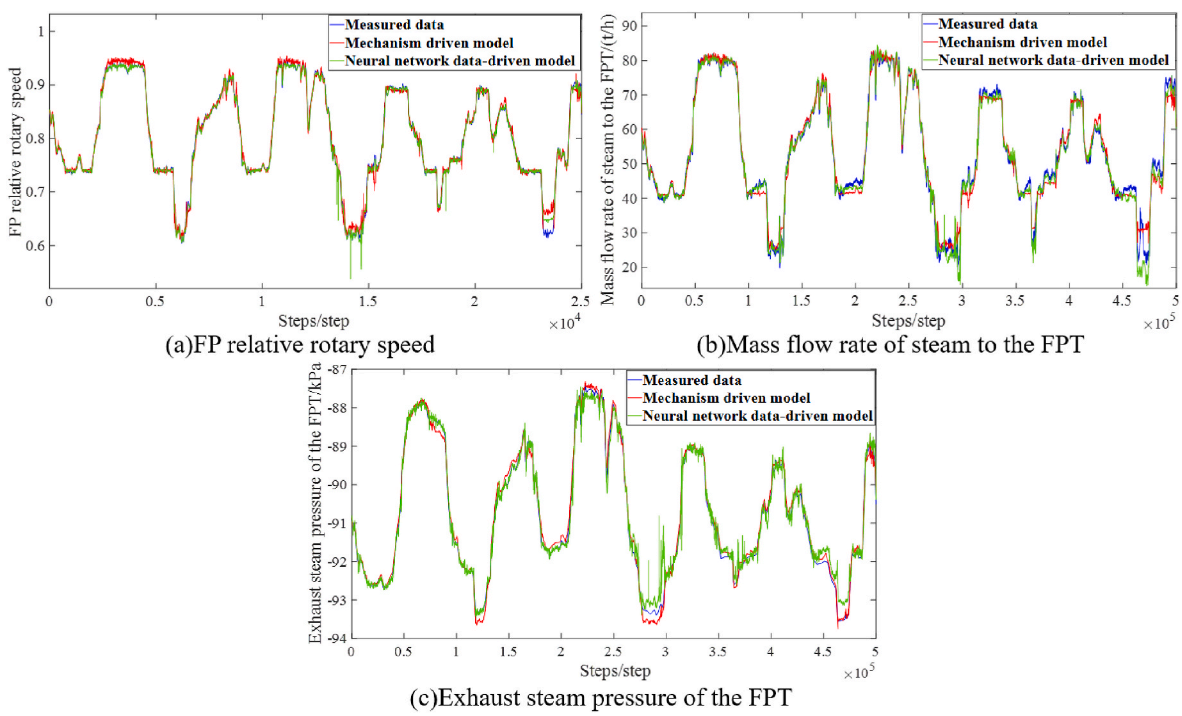

Fig. 8. Parameters predicted by both the mechanism data hybrid driven models and neural network data-driven model.

then increases, and the enthalpy of the LPT exhaust steam decreases initially and then increases. Consequently, the work done per unit mass of live steam follows a pattern of initial increase and subsequent decrease. Comparing the two datasets, a higher circulating water inlet temperature leads to higher exhaust steam pressure and, consequently, higher exhaust steam enthalpy. While other parameters exhibit minor differences, the higher exhaust steam enthalpy results in a decrease in the work done per unit mass of live steam. Overall, the trends in the exhaust steam enthalpy and work done per unit mass of live steam align with the design values. However, the exhaust steam enthalpy in operation surpasses the design value, while the work done per unit mass of live steam is lower than the design value. On average, the LPT exhaust steam enthalpy is 3.13 % higher, and the work done per unit mass of live steam is 5.05 % lower than the design values.

The heat absorption per unit mass of live steam and STS energy efficiency are depicted in Fig. 10 (e) and (f). The enthalpy of the boiler feedwater increases with the unit load, so the heat absorption per unit mass of live steam decreases with the increase of the unit load. Within the load range of 30 %–75 %, the increase in work done per unit mass of live steam, coupled with the decrease in heat absorption per unit mass of live steam, leads to a rapid improvement in STS energy efficiency. However, when the load exceeds 75 %, the increase in exhaust enthalpy results in a slight decrease in STS energy efficiency. There is minimal difference between the two datasets in terms of heat absorption per unit mass of live steam, so the lower work done per unit mass of live steam in the green dataset also contributes to lower efficiency. Overall, both parameters exhibit the same variation pattern as the design values but fall short of the design values. The heat absorption per unit mass of live steam is 1.19 % less than the design value, and the STS energy efficiency is relatively 3.89 % lower than the design value. The efficiency is lower than the design value due to performance degradation.

Fig. 11 illustrates the relative deviations from the design values for key parameters, including LPT exhaust steam enthalpy, work done, heat absorption per unit mass of live steam, and STS energy efficiency. These deviations become more significant as the unit load increases. Regardless of the load range, the operational STS energy efficiency is consistently lower than the design value. The maximum deviation of −5.00 % occurs at 1039.37 MW, while the minimum deviation of −3.02 % is observed at 779.51 MW. These deviations highlight the real-world challenges in achieving idealized design performance, particularly as the unit load varies.

Fig. 12 displays the parameter deviations under different cold-end

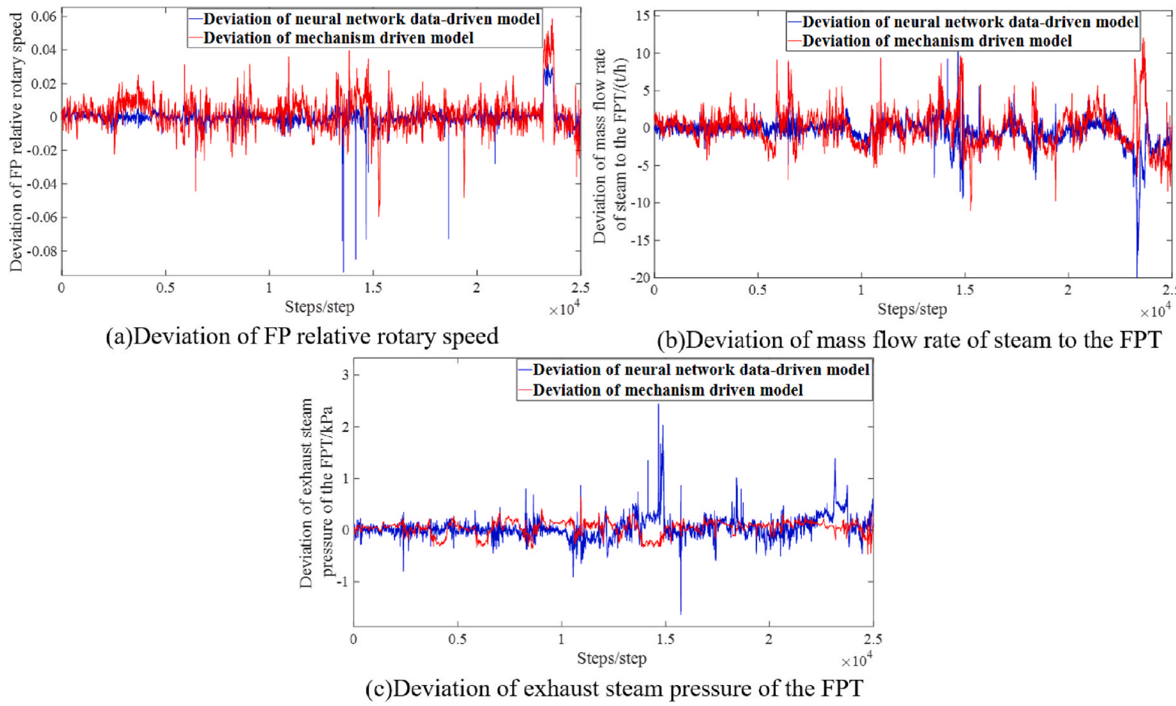

Fig. 9. Deviation between measured and simulation values of two models.

Table 1
Model accuracy analysis.

Simulation parameters	Model type	Mean absolute error (MAE)	Root-mean-square error (RMSE)	Determinate coefficient (R^2)
FP relative rotary speed	Neural network data-driven model	0.0026	0.0048	0.9972
	Mechanism data hybrid driven model	0.0069	0.0101	0.9878
Mass flow rate of steam to the FPT	Neural network data-driven model	1.0809 t/h	1.8573	0.9873
	Mechanism data hybrid driven model	1.7397 t/h	2.3682	0.9793
Exhaust steam pressure of the FPT	Neural network data-driven model	0.1367 kPa	0.2141	0.9841
	Mechanism data hybrid driven model	0.1165 kPa	0.1395	0.9933

conditions characterized by circulating water inlet temperatures of 4.5 ± 1 °C and 6.5 ± 1 °C. Comparing the two conditions, it is observed that the LPT exhaust steam enthalpy is 0.41 % lower at the lower circulating water inlet temperature, while the work done per unit mass of live steam is 0.44 % higher. Consequently, the STS energy efficiency is 0.45 % higher under the lower circulating water inlet temperature condition. Notably, there is no significant difference in the heat absorption per unit mass of live steam between the two conditions.

As the operational time of the unit increases, the system and equipment of the unit naturally experience aging, leading to the degradation of unit performance. Consequently, there is a discernible difference between the operational values and the design values. In summary, when comparing different circulating water inlet temperatures, the lower circulating water inlet temperature results in a lower LPT exhaust steam pressure, assuming the same number of circulating pumps are in service. This lower exhaust steam pressure leads to reduced exhaust steam enthalpy. Under equivalent heat absorption conditions, a lower exhaust steam enthalpy allows for greater work done per unit mass of live steam, signifying higher steam turbine efficiency.

3.3. Operation optimization based on digital twin models

The improvement of STS energy efficiency can be achieved through the judicious adjustment of heat source and heat sink parameters. In the context of the heat source, the analysis in this section will focus on the effect of live steam pressure on the heat absorption process. Regarding the heat sink, the optimization of circulating pump scheduling will be explored to attain optimal operation of the cold end.

3.3.1. Live steam pressure optimization

The analysis in this section further explores the effect of different circulating water inlet temperatures, as discussed in Section 3.2, on the feedwater mass flow rate and water-coal ratio. The comparisons of these parameters are illustrated in Fig. 13 (a) and (b). It is observable that the feedwater mass flow rate increases with the rise in unit load. In accordance with Eq. (21), the water-coal ratio decreases with the increase of the heat absorption per unit mass of live steam. The heat absorption per unit mass of live steam decreases with the increase of the unit load, resulting in an increase in the water-coal ratio.

In summary, the trends in the variation of both parameters align with the design values. However, it should be noted that the calculated feedwater mass flow rate is, on average, 6.99 % higher than the design value, and the water-coal ratio is 1.35 % higher than the design value. There are several factors contributing to the larger water-coal ratio observed in actual operation, including equipment aging and higher condenser back pressure, among others.

The feedwater mass flow rate fitting curves for the two datasets are depicted in Fig. 13(c) and (d), respectively, and the analytical formula is as follows:

$$m_{\mathrm{w1}} = 0.0004314 W_{\mathrm{e}}^{2} + 0.2093 W_{\mathrm{e}} + 171, T_{\mathrm{cwi}} = 4.5 \pm 1^{\circ}C \quad (23)$$

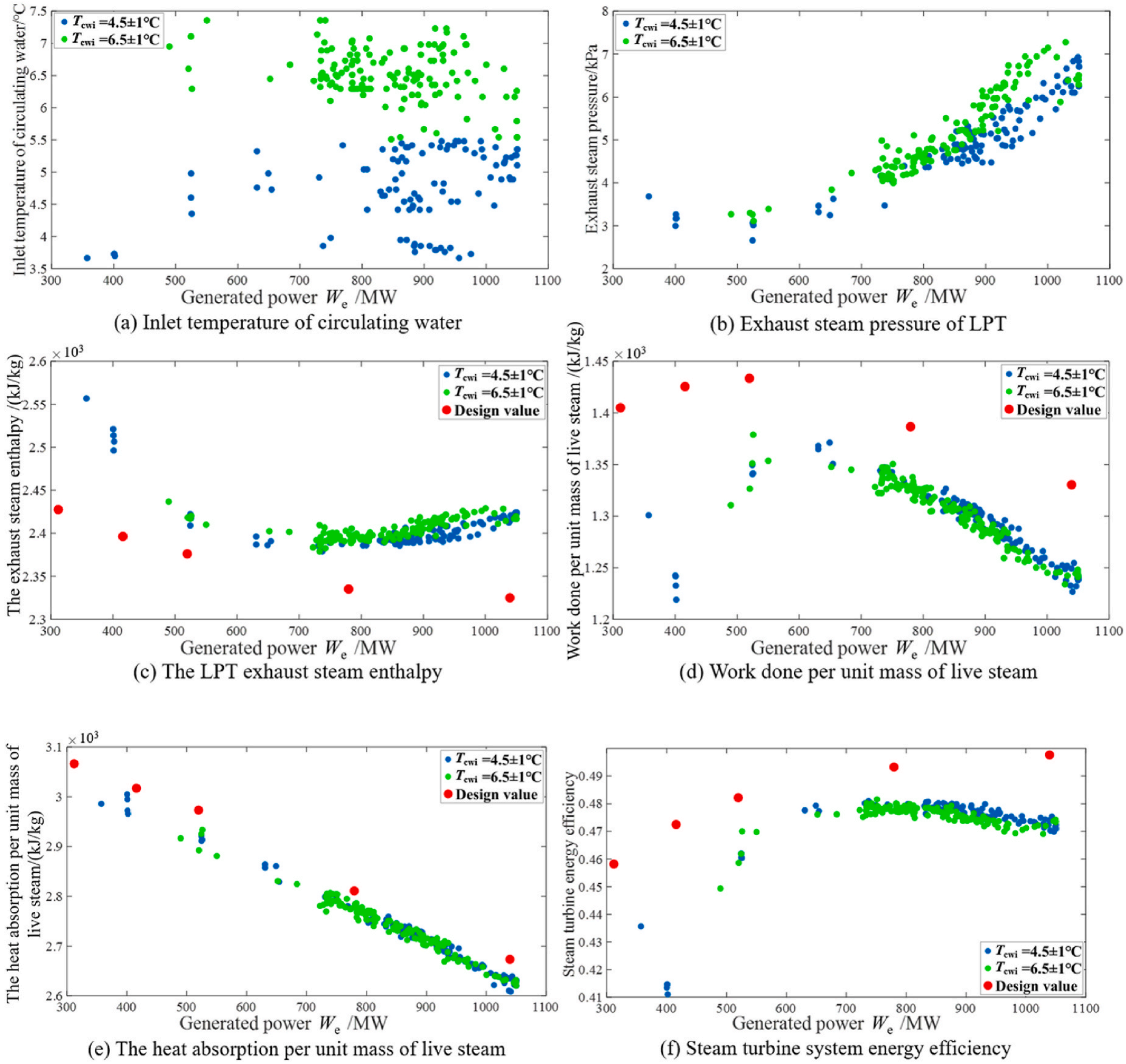

Fig. 10. STS energy efficiency diagnosis with different circulating water inlet temperatures.

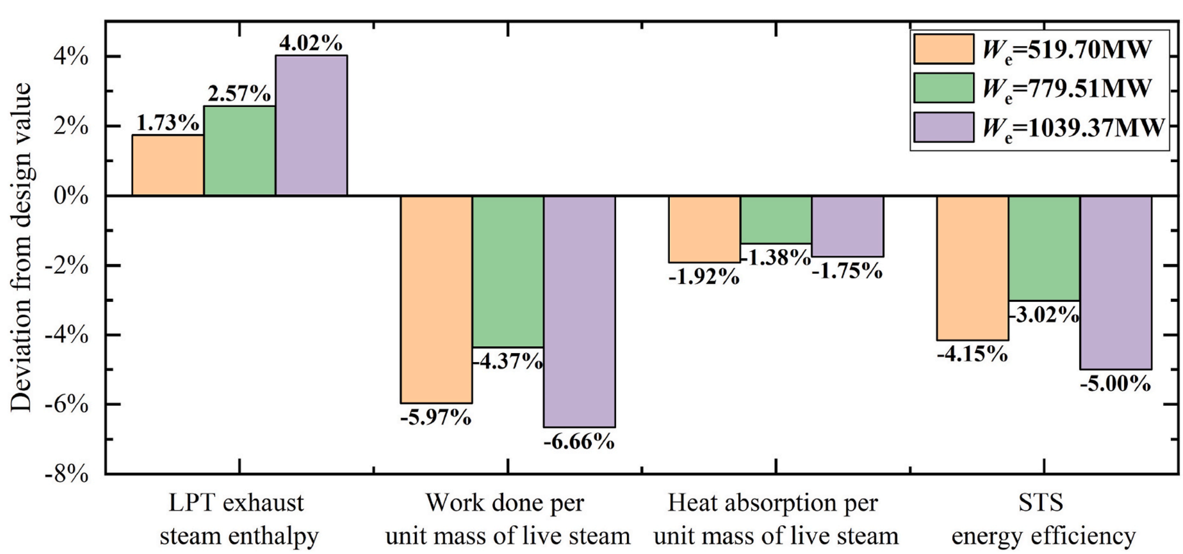

Fig. 11. The deviation from the design value of different parameters.

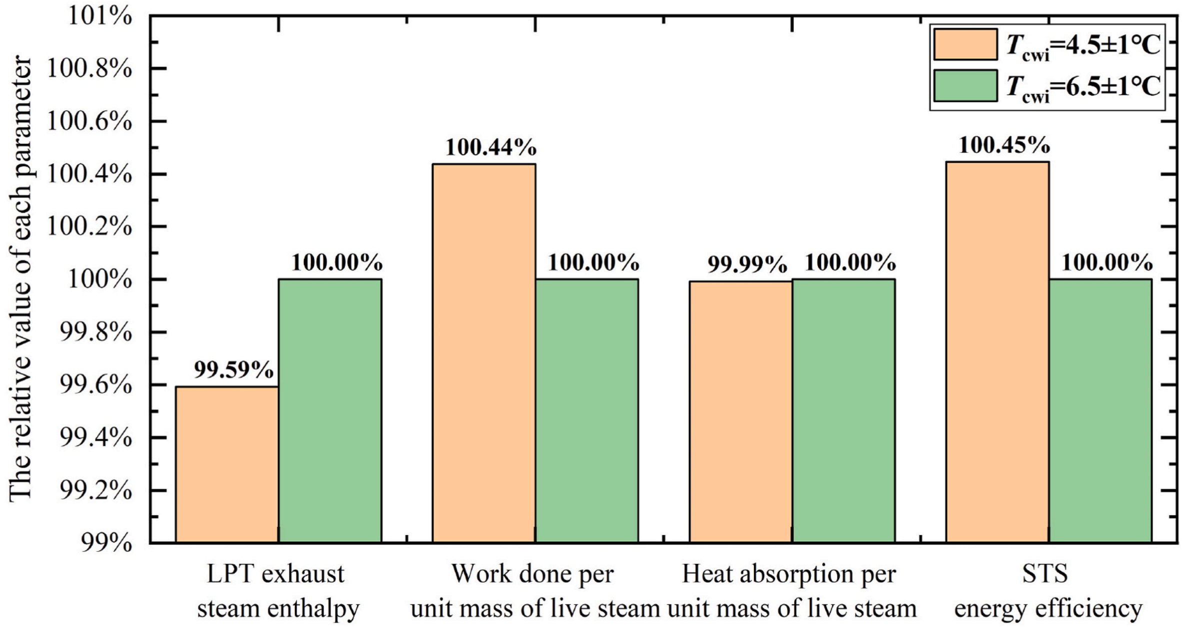

Fig. 12. The parameter deviations under different cold end conditions.

$$m_{w2} = 0.0003741W_e^2 + 0.3072W_e + 133.2, T_{cwi} = 6.5 \pm 1^\circ C \tag{24}$$

The water-coal ratio should be precisely regulated to facilitate the efficient operation of the unit. The water-coal ratio fitting curves for the two datasets are presented in Fig. 13(e) and (f), respectively, and the analytical equation is as follows:

$$\lambda_1 = 6.995 \times 10^{-7}W_e^2 + 0.0009158W_e + 8.771, T_{cwi} = 4.5 \pm 1^\circ C \tag{25}$$

$$\lambda_2 = 6.498 \times 10^{-7}W_e^2 + 0.0009023W_e + 8.831, T_{cwi} = 6.5 \pm 1^\circ C \tag{26}$$

As one of the crucial thermal parameters of the STS, optimizing the live steam pressure can maximize energy efficiency. The live steam pressure optimization is carried out while maintaining unchanged external operating conditions, the STS cold-end system's operating scheme, and the configuration of the STS feedwater regenerative thermal system. The primary objective of this optimization is to identify the live steam pressure that yields the highest STS energy efficiency within different load ranges. Consequently, determining the optimal live steam pressure for each load range is essential for achieving maximum efficiency. This determination is accomplished with the assistance of the feedwater mass flow rate curve and water-coal ratio curve, as illustrated in Fig. 14. Fig. 14(a) depicts the STS energy efficiency corresponding to different load ranges and various live steam pressures. By comparing the STS energy efficiency values associated with different live steam pressures within the same load range in the figure, we can identify the optimal live steam pressure for each load range. The resulting optimization curve for live steam pressure is presented in Fig. 14(b).

Following the optimization of live steam pressure, there is a notable improvement in STS energy efficiency. Fig. 15 illustrates the relative increase in STS energy efficiency resulting from live steam pressure optimization. Considering the four load points with the most historical operating data and comparing them with the minimum efficiency and average efficiency of the same load range, the efficiency after operational optimization exhibits an average increase of 0.78 % and 0.35 %, respectively.

3.3.2. Cold end system optimization

The core of cold end optimization lies in determining the number of circulating pumps in operation to achieve the highest STS net efficiency. The optimization of the cold end system is based on constant constraints, including the operating mode of live steam pressure in the STS and the configuration of the STS feedwater regenerative thermal system. The optimization objective remains to attain the highest STS energy efficiency. The method employed involves exploring the most suitable cold end system circulating pump scheduling schemes for different load ranges to correspond with the optimum STS energy efficiency. The data used for the circulating water inlet temperature ranges from 3.5 to 7.5 °C, and during this range, only one circulating pump is in service. Data for a circulating water inlet temperature of 15–17 °C are included for comparison, where two circulating pumps are in service. The following is an energy efficiency comparative analysis of circulating pump numbers under different circulating water inlet temperatures and different loads.

The comparisons of the circulating water inlet temperature, LPT exhaust steam pressure, exhaust steam enthalpy, and work done per unit mass of live steam are shown in Fig. 16(a), (b), (c), and (d). Lower exhaust pressure and enthalpy can be achieved for the cold end system with two circulating pumps compared with that with one circulating pump, which leads to a higher work done per unit mass of live steam.

The heat absorption per unit mass of live steam, steam turbine efficiency, and equivalent steam turbine efficiency, accounting for the power consumption deviation of the circulating pump, are illustrated in Fig. 16(e), (f), and (g). There is no significant difference in heat absorption between them. Regardless of whether the circulating pump power consumption is considered, because of the higher work done per unit mass of live steam, the STS energy efficiency of the data with two circulating pumps in service is higher at high loads than the data with only one circulating pump in service. Nevertheless, when compared to the design efficiency, a certain discrepancy persists.

Utilizing various scheduling schemes for circulating pumps, we selected four load points ranging from 700 MW to 1100 MW to assess the STS energy efficiency deviation between the two datasets within the same load range. As depicted in Fig. 17, the deviation in the overall dataset escalates with increasing load. The operation optimization of cold end system is to balance the tradeoff between the energy consumption of circulating pumps and the steam turbine output power. When the power load is 740 MW, the STS energy efficiency is higher for the cold end system with one circulating pump. However, when the power load is over 840 MW, the STS energy efficiency is higher for the cold end system with two circulating pumps, because the increase of

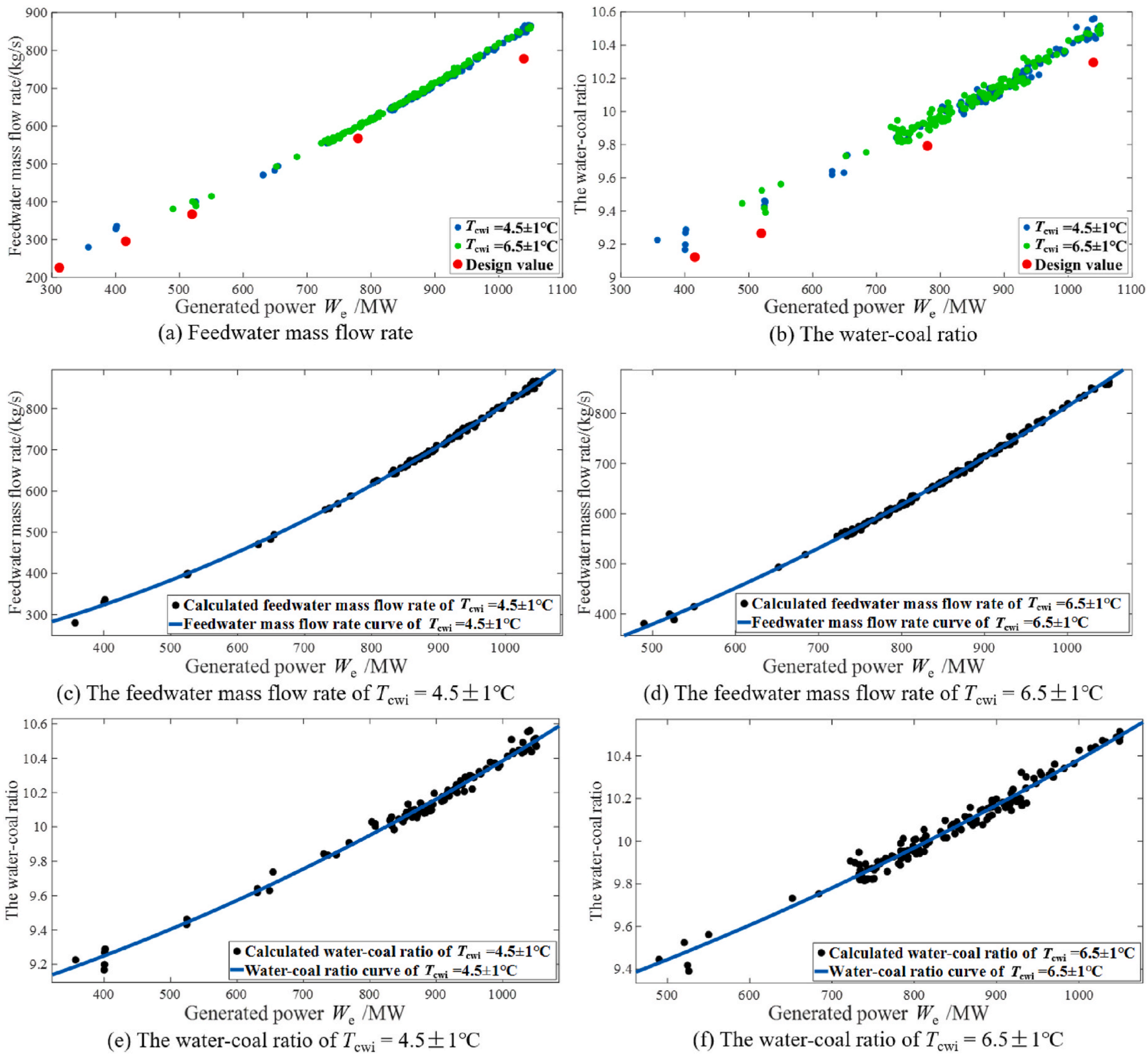

Fig. 13. Feedwater mass flow rate and water-coal ratio with different T_{cwi}.

steam turbine output power is over the energy consumption of an added circulating pump.

The comparisons between the feedwater mass flow rate and the water-coal ratio in the two datasets are elucidated in Fig. 18(a) and (b). Under high load conditions, the heightened cooling efficiency results in a reduction in the LPT exhaust steam enthalpy, consequently enhancing the work done per unit mass of live steam. Consequently, the green dataset necessitates a lower feedwater mass flow rate for the same power output. It is essential to highlight that the water-coal ratio curves for both datasets exhibit almost indistinguishable profiles, and both surpass the designated values.

In Fig. 18(c) and (d), the fitting curves for the feedwater mass flow rate and water-coal ratio are presented for the dataset with two circulating pumps in operation. The analytical formulations for these curves are as follows:

$$m_{wh} = 0.0003128 W_e^2 + 0.3963 W_e + 98.15 \tag{27}$$

$$\lambda_h = 5.871 \times 10^{-7} W_e^2 + 0.00103 W_e + 8.761 \tag{28}$$

Following the aforementioned analysis, it is evident that the energy efficiency of the two datasets varies across distinct load ranges, emphasizing the existence of an optimal circulating pump scheduling scheme. Consequently, we focus on the load range of 600 MW–1100 MW, which is common to both datasets, to evaluate the equivalent STS energy efficiency within this range. As illustrated in Fig. 19, two curves intersect at STS output power of 780 MW. When the load is below 780 MW, running a single circulating pump results in higher STS energy efficiency, while when the load surpasses 780 MW, operating two circulating pumps yields greater equivalent STS energy efficiency. Notably, it is worth mentioning that in actual operation, the load intersection point will be further advanced due to the lower circulating water inlet temperature observed in the single pump scheme employed in this study.

Fig. 20 depicts the relative enhancement of STS energy efficiency resulting from cold end optimization. Across the five load points ranging from 640 MW to 1040 MW, the maximum observed relative increase in energy efficiency post-optimization is 0.34 %, while the minimum observed relative increase stands at 0.01 %. On average, there is a 0.14 % increase in energy efficiency.

Consequently, in the practical operation of thermal power plants, optimizing the circulating pump scheduling scheme across the entire load range, including loads below 600 MW, and implementing this optimized scheme (which is highly feasible) can result in a more substantial enhancement in STS energy efficiency across the entire load spectrum, surpassing an average relative improvement of 0.14 %.

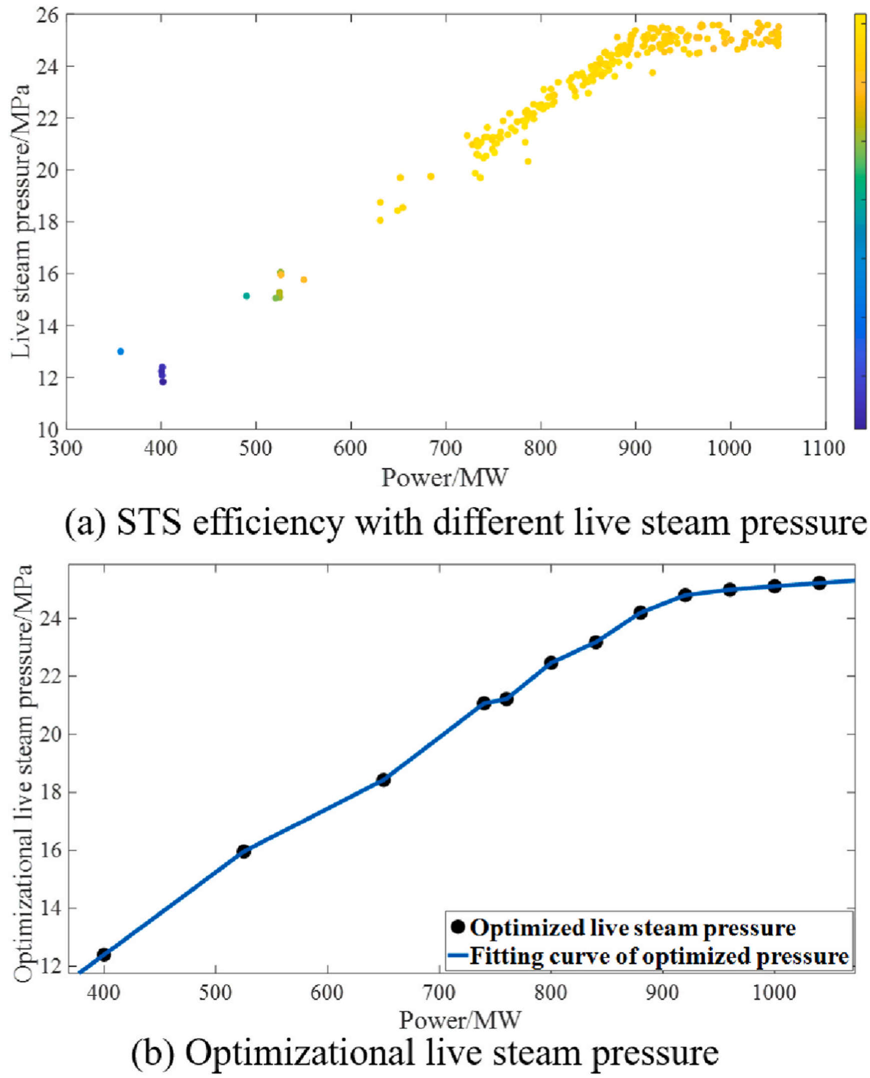

Fig. 14. Live steam pressure optimization.

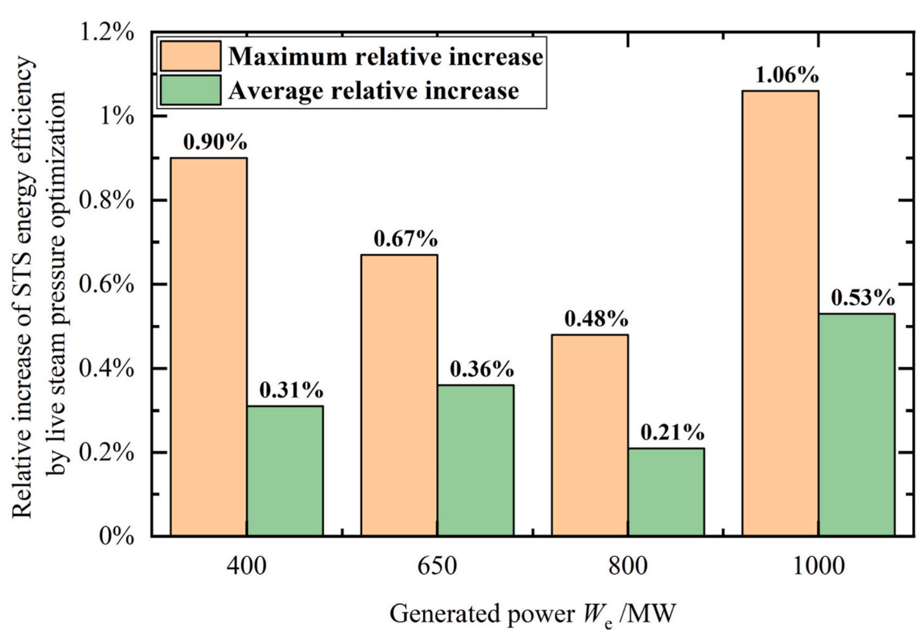

Fig. 15. The relative increase in STS energy efficiency by live steam pressure optimization.

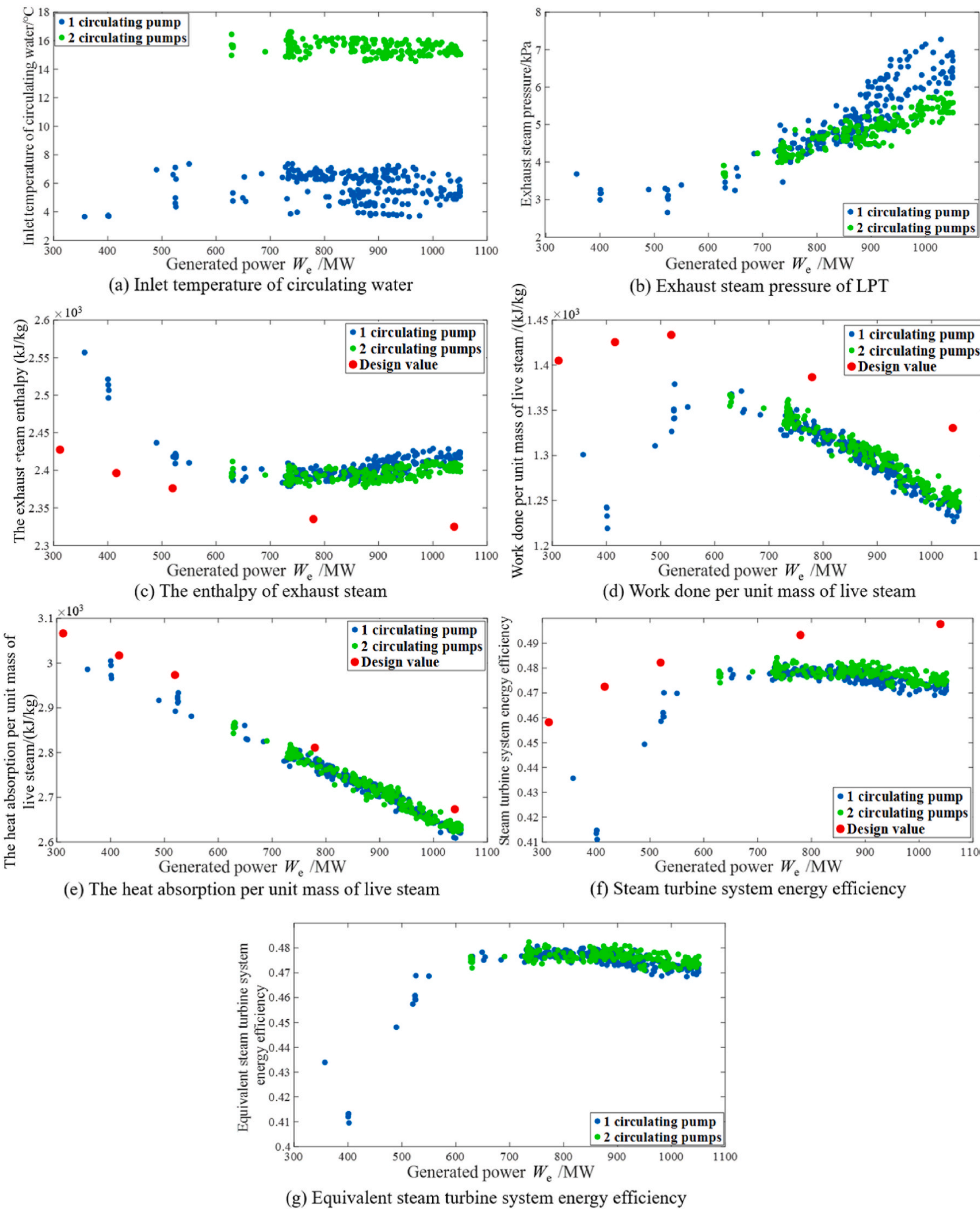

Fig. 16. STS energy efficiency diagnosis with different numbers of circulating pumps in service.

4. Conclusion

Due to the increasing prevalence of renewable power sources, thermal power plants experience a reduction in energy efficiency, especially when providing peak regulation services. Among the vital components of a thermal power plant, the STS holds primary importance, comprising steam turbines (HPT, IPT, LPT, and FPT), regenerative heaters (No.1 to No.8 RHs), and pumps (CP, BP, and FP). It significantly influences the energy efficiency of the entire thermal power plant. Consequently, digital twin modeling has been employed to assess the energy efficiency of STSs, utilizing both mechanism-driven and data-driven modeling methods.

The digital twin parameters for STS are primarily developed within the FP subsystem, which serves as the core of STS. Subsequently, essential digital twin parameters are simulated following the selection of appropriate modeling methods. Among these parameters, the BP outlet pressure, feedwater mass flow rate of the FP, feedwater pressure at the FP outlet, FP efficiency, FP power, and FPT exhaust steam pressure are simulated using the mechanism data hybrid driven modeling method, ensuring precision. Additionally, the FP relative rotary speed and the mass flow rate of steam to the FPT are simulated using neural network data-driven modeling methods to achieve high accuracy.

Based on these digital twin parameters, an energy efficiency analysis model for STS with varying cold end parameters is developed through

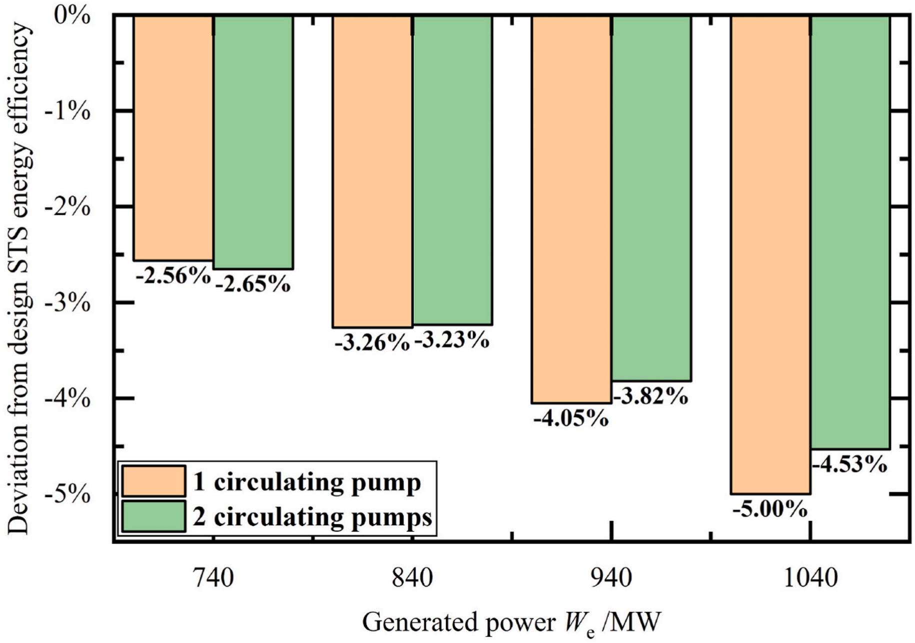

Fig. 17. The deviation from the design STS energy efficiency under different cold end conditions.

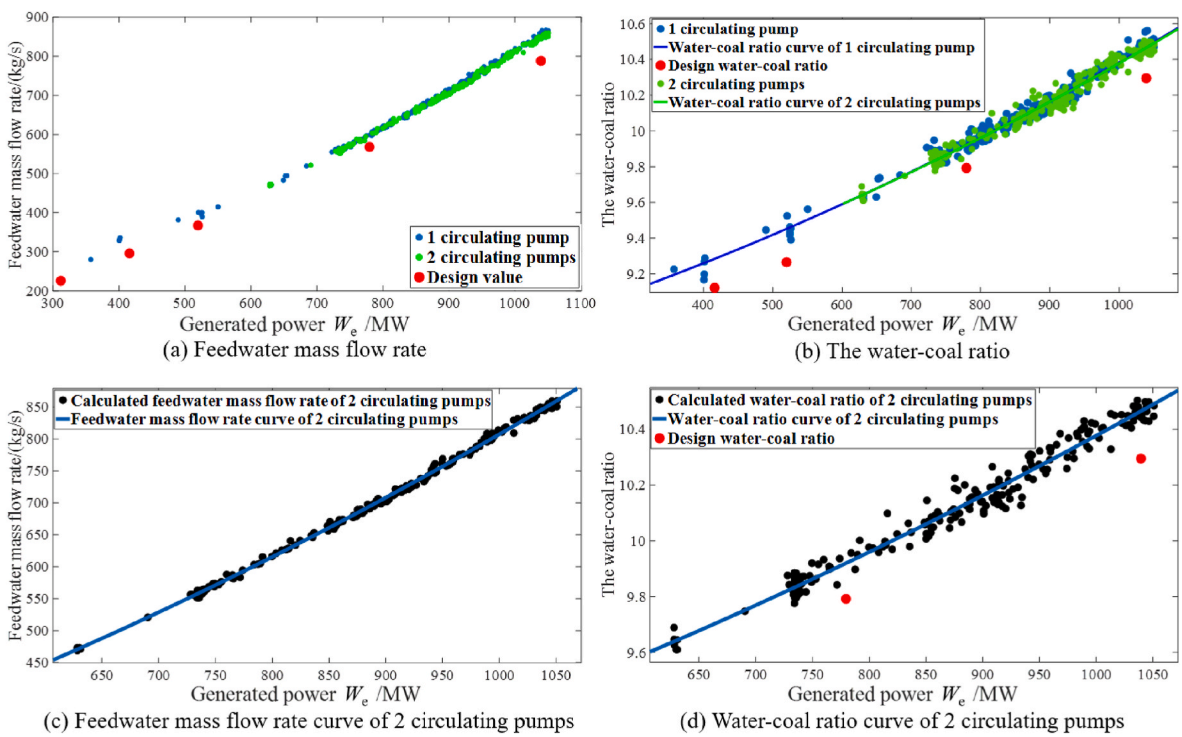

Fig. 18. Feedwater mass flow rate and water-coal ratio with different circulating pump numbers.

the mechanism-driven modeling method. This model includes critical factors such as LPT exhaust steam enthalpy, work done per unit mass of live steam, heat absorption per unit mass of live steam, STS energy efficiency, feedwater mass flow rate, and water-coal ratio. The analysis reveals that, on average, a lower circulating water inlet temperature results in a 0.45 % increase in STS energy efficiency relative to a higher circulating water inlet temperature. However, the operational energy efficiency remains, on average, 3.89 % lower than the design value. Additionally, the relationship curve between the water-coal ratio and load, obtained from the energy efficiency analysis model of STS, holds significant value for guiding unit operation optimization.

Subsequently, optimizations in live steam pressure and the cold end system of the thermal power plant are executed, leading to the derivation of optimal operation curves for live steam pressure and optimal scheduling schemes for circulating water pumps. Following these optimizations, the STS energy efficiency can be improved by 0.35 % and 0.14 % relatively on average.

In summary, leveraging the digital twin parameters of the FP subsystem, the energy efficiency digital twin analysis model of STS developed in this study proves to be a valuable tool for accurately evaluating

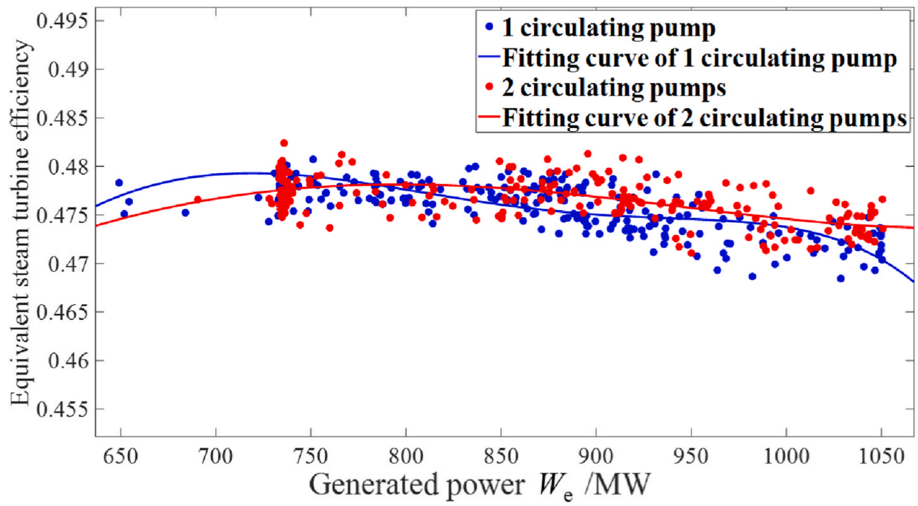

Fig. 19. Optimization of the circulating pump number in operation.

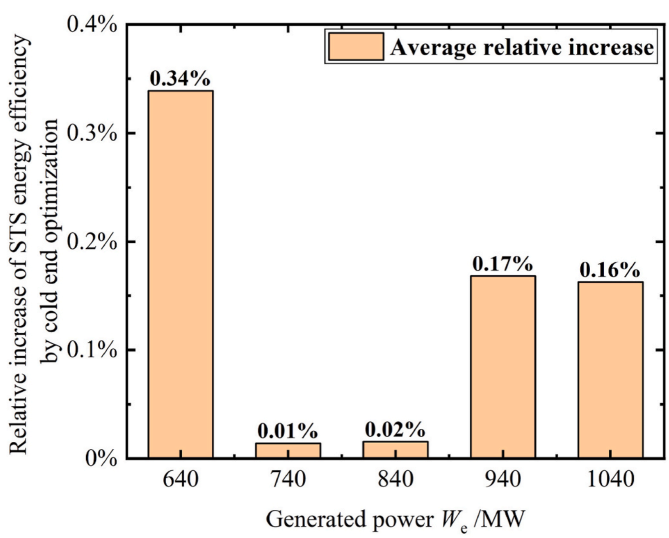

Fig. 20. The relative increase in STS energy efficiency by cold end optimization.

and diagnosing STS energy efficiency. It also facilitates the analysis of how the circulating water inlet temperature influences the STS energy efficiency and contributes to optimizing the live steam pressure and the cold end system. The on-line self-learning should be considered in future study, which is also the limitations of the applied approach in this paper.

CRediT authorship contribution statement

Chen Chen: Methodology, Writing - original draft. **Ming Liu:** Methodology, Supervision, Writing - review & editing. **Mengjie Li:** Methodology. **Yu Wang:** Data curation, Methodology. **Chaoyang Wang:** Supervision. **Junjie Yan:** Methodology, Supervision, Writing - review & editing.

Declaration of competing interest

The authors declare that they have no known competing financial interests or personal relationships that could have appeared to influence the work reported in this paper.

Data availability

Data will be made available on request.

Acknowledgments

This work was supported by the Natural Science Foundation of China (Grant Number 52022079) and the Energy Security Technology Research Project of Huaneng Group Science and Technology Foundation (Grant Number HNKJ20-H87).

Appendix A. Supplementary data

Supplementary data to this article can be found online at https://doi.org/10.1016/j.energy.2023.129969.

References

[1] Md K, Abu M, Mohammad K, Firdaus MS, Siti AB, Nazmi S, et al. Energy revolution for our common future: an evaluation of the emerging international renewable energy law. Energies 2018;11:1769.
[2] Wang G, Liao Q, Li Z, Zhang H, Liang Y, Wei X. How does soaring natural gas prices impact renewable energy: a case study in China. Energy 2022:252.
[3] Hongtao L, Wenjia L. The analysis of effects of clean energy power generation. Energy Proc 2018;152:947–52.
[4] Johnson N, Krey V, McCollum DL, Rao S, Riahi K, Rogelj J. Stranded on a low-carbon planet: implications of climate policy for the phase-out of coal-based power plants. Technol Forecast Soc Change 2015;90:89–102.
[5] Liu M, Wang S, Yan J. Operation scheduling of a coal-fired CHP station integrated with power-to-heat devices with detail CHP unit models by particle swarm optimization algorithm. Energy 2021;214:119022.
[6] Liu M, Wang S, Zhao Y, Tang H, Yan J. Heat–power decoupling technologies for coal-fired CHP plants: operation flexibility and thermodynamic performance. Energy 2019;188:116074.
[7] Liu M, Zhang X, Ma Y, Yan J. Thermo-economic analyses on a new conceptual system of waste heat recovery integrated with an S-CO2 cycle for coal-fired power plants. Energy Convers Manag 2018;161:243–53.
[8] Zhao Y, Fan P, Liu M, Chong D, Yan J. Fatigue lifetime estimation of a heater in coal-fired power plants under a flexible operational framework-regulating extraction steam of high-pressure heaters. Energy Proc 2019;158:5225–30.
[9] Sleiti AK, Kapat JS, Vesely L. Digital twin in energy industry: proposed robust digital twin for power plant and other complex capital-intensive large engineering systems. Energy Rep 2022;8:3704–26.
[10] Walton ALJ, Tomovic CL, Grieves MW. Product lifecycle management: measuring what is important - product lifecycle implementation maturity model. In: Bernard A, Rivest L, Dutta D, editors. Product lifecycle management for society (plm 2013), vol. 409. Berlin: Springer-Verlag Berlin; 2013. p. 406–21.
[11] Grieves M. Digital twin: manufacturing excellence through virtual factory replication. 2015.
[12] Tao F, Cheng J, Qi Q, Zhang M, Zhang H, Sui F. Digital twin-driven product design, manufacturing and service with big data. Int J Adv Des Manuf Technol 2018;94: 3563–76.

[13] Grieves M. Virtually intelligent product systems: digital and physical twins. 2019. p. 175–200.
[14] Alobaid F, Mertens N, Starkloff R, Lanz T, Epple B. Progress in dynamic simulation of thermal power plants. Prog Energy Combust Sci 2017;59:79–162.
[15] Mao M, Xiao H. Study on key technologies of optimization of big data for thermal power plant performance. In: You Z, Xiao J, Tan Z, editors. Materials science, energy technology and power engineering II (MEP2018), vol. 1971. Melville: Amer Inst Physics; 2018, 030015.
[16] Huang TE, Guo Q, Sun H. A distributed computing platform supporting power system security knowledge discovery based on online simulation. IEEE Trans Smart Grid 2016;8:1. –1.
[17] Wang NL, Zhang Y, Zhu LF, Yang ZP. Operation optimization approaches of thermal power units with big data-driven hybrid modeling. Appl Mech Mater 2014; 631–632:362–6.
[18] Zhao Y, Wang C, Liu M, Chong D, Yan J. Improving operational flexibility by regulating extraction steam of high-pressure heaters on a 660 MW supercritical coal-fired power plant: a dynamic simulation. Appl Energy 2018;212:1295–309.
[19] Zhao Y, Liu M, Wang C, Li X, Chong D, Yan J. Increasing operational flexibility of supercritical coal-fired power plants by regulating thermal system configuration during transient processes. Appl Energy 2018;228:2375–86.
[20] Alobaid F, Ströhle J, Epple B, Kim H-G. Dynamic simulation of a supercritical once-through heat recovery steam generator during load changes and start-up procedures. Appl Energy 2009;86:1274–82.
[21] Tian Yuan, Zhang JQ, Wang JC. Online performance monitoring platform based on the whole process models of subcritical coal-fired power plants. Appl Therm Eng 2017;124:1368–81. 2017.
[22] Hentschel J, Zindler H, Spliethoff H. Modelling and transient simulation of a supercritical coal-fired power plant: dynamic response to extended secondary control power output. Energy 2017;137:927–40.
[23] Si-ke H, Hui-fen G, Xue-jing J. Regulating characteristics analysis of boiler feed-water pump when 600MW unit sliding-pressure operating. Energy Proc 2012;17: 1153–60.
[24] Sonawat A, Kim S, Ma S-B, Kim S-J, Lee JB, Yu MS, et al. Investigation of unsteady pressure fluctuations and methods for its suppression for a double suction centrifugal pump. Energy 2022;252:124020.
[25] Spence R, Amaral-Teixeira J. A CFD parametric study of geometrical variations on the pressure pulsations and performance characteristics of a centrifugal pump. Comput Fluid 2009;38:1243–57.
[26] Qiu J, Lin Y. Transient simulation modeling of condenser based on thermal system dynamics. In: Proceedings of the 25TH international conference on nuclear engineering, vol. 6. New York: Amer Soc Mechanical Engineers; 2017, V006T08A115. 2017.
[27] Wang C, Liu M, Zhao Y, Qiao Y, Chong D, Yan J. Dynamic modeling and operation optimization for the cold end system of thermal power plants during transient processes. Energy 2018;145:734–46.
[28] Zima W, Nowak-Oconń M, Oconń P. Novel online simulation-ready models of conjugate heat transfer in combustion chamber waterwall tubes of supercritical power boilers. Energy 2018;148:809–23.
[29] Xiang Z, Yuan J, Xu L, Tian Z, Wang J. Pseudo-online optimization of condenser pressure for the cold-end system with variable speed pumps. Appl Therm Eng 2017;126:339–49.
[30] Runvik H. Modelling and start-up optimization of a coal-fired power plant. Technology & Engineering; 2014.
[31] Liu Z, Karimi IA. Simulation and optimization of a combined cycle gas turbine power plant for part-load operation. Chem Eng Res Des 2018;131:29–40.
[32] Anjum H, Ul-Haq A, Mahmood I. Dynamic modeling and heat flow study of a thermal power plant using OpenModelica. IEEE Access 2020;8:178614–26.
[33] Wang Z, Liu M, Yan J. Flexibility and efficiency co-enhancement of thermal power plant by control strategy improvement considering time varying and detailed boiler heat storage characteristics. Energy 2021:232.
[34] Wang Q, Pan L, Lee KY, Wu Z. Deep-learning modeling and control optimization framework for intelligent thermal power plants: a practice on superheated steam temperature. Kor J Chem Eng 2021;38:1983–2002.
[35] Wang C, Zhao Y, Liu M, Qiao Y, Chong D, Yan J. Peak shaving operational optimization of supercritical coal-fired power plants by revising control strategy for water-fuel ratio. Appl Energy 2018;216:212–23.
[36] Yin J, Liu M, Zhao Y, Wang C, Yan J. Dynamic performance and control strategy modification for coal-fired power unit under coal quality variation. Energy 2021; 223:120077.
[37] Liu M, Wang S, Zhao Y, Tang H, Yan J. Heat–power decoupling technologies for coal-fired CHP plants: operation flexibility and thermodynamic performance. Energy 2019;188:116074.
[38] Liangyu M, Xinhui D, Xian G, Jin M. A study on real-time simulation mathematical model of variable speed boiler feedwater pump. JOURNAL OF NORTH CHINA ELECTRIC POWER UNIVERSITY; 1998.
[39] Jianqun X, Runtian G, Keyi Z. A new type of universal mathematical model of feed water pump. TURBINE TECHNOLOGY; 1999.
[40] Liu MF, Lu GL. The efficiency analysis of steam turbine-driven feed water pump. Appl Mech Mater 2013;401–403:312–5.
[41] Mrzljak V, Poljak I, Mrakovčić T. Energy and exergy analysis of the turbo-generators and steam turbine for the main feed water pump drive on LNG carrier. Energy Convers Manag 2017;140:307–23.
[42] Shlens J. A tutorial on principal component analysis. Int J Rem Sens 2014;51.
[43] Strušnik D, Avsec J. Exergoeconomic machine-learning method of integrating a thermochemical Cu–Cl cycle in a multigeneration combined cycle gas turbine for hydrogen production. Int J Hydrogen Energy 2022;47:17121–49.
[44] Strušnik D. Integration of machine learning to increase steam turbine condenser vacuum and efficiency through gasket resealing and higher heat extraction into the atmosphere. Int J Energy Res 2022;46:3189–212.
[45] Strušnik D, Avsec J. Artificial neural networking and fuzzy logic exergy controlling model of combined heat and power system in thermal power plant. Energy 2015; 80:318–30.
[46] Yu F, Xu X. A short-term load forecasting model of natural gas based on optimized genetic algorithm and improved BP neural network. Appl Energy 2014;134: 102–13.